J Mater Sci (2016) 51:50–70
DOI 10.1007/s10853-015-9389-y

50TH ANNIVERSARY

A review of phase equilibria in Heusler alloy systems containing Fe, Co or Ni

Ming Yin[1] · John Hasier[1] · Philip Nash[1]

Received: 18 June 2015 / Accepted: 26 August 2015 / Published online: 10 September 2015
© Springer Science+Business Media New York 2015

Abstract The phase equilibria associated with Heusler-type intermetallic compounds have been reviewed for systems containing Fe, Co or Ni. Ternary alloy systems are identified in which the phase equilibria are not well established or completely unknown and which are therefore prime targets for additional experimental work. Other systems in which there is conflicting information regarding the existence of a Heusler phase are also identified. Design issues are highlighted in terms of phase combinations that may benefit functional properties or processing of bulk material containing Heusler compounds.

Introduction

Since the discovery of the first Heusler compounds, Cu_2Mn(Al, Sn, Zn, Bi, Sb or B), by Heusler in 1903 [1], a large number of intermetallic compounds of the type X_2YZ have been discovered. However, not all compounds of this stoichiometry have the original prototype Cu_2MnAl ($L2_1$, prototype Cu_2MnAl, Pearson symbol cF16, space group $Fm\ \bar{3}m$) structure. Typically, the X and Y elements are transition elements and the Z element is from Group III–V in the periodic table, although there are exceptions, Fig. 1. On this basis, there are potentially thousands of such compounds. While for decades after their discovery, these intermetallics were little more than a scientific curiosity, studied mostly for their ferromagnetic properties, in the last 25 years there is growing interest in other functional properties [2]. These include magnetic shape memory and magneto-caloric effects, thermoelectric properties and spintronic behaviour amongst others [3–6]. For some properties, a deviation from stoichiometry can lead to property changes due to the presence of constitutional defects, or changes can be produced by fourth element substitution [7, 8]. This allows the properties to be tuned to optimum values for a specific application.

In order to design materials based on, or incorporating, Heusler compounds it is necessary to understand the phase equilibria in the ternary systems in which they occur. However, while many papers deal with the properties of stoichiometric Heusler phases or predictions of their stability, there is a lack of ternary phase diagram data for alloy systems containing Heusler phases. Where there are phase equilibria data they are often confined to a single isothermal section, because experimental phase diagram studies are very time consuming. In some cases, the phase diagrams available contradict the results of single composition determinations of the presence of a Heusler phase. Computational thermodynamics utilizing the Calphad approach can be used to generate phase diagrams in a more efficient way than experiments and therefore offer an efficient method to investigate phase relationships. Nevertheless, some experimental data are needed such as equilibrium phase compositions, transition temperatures and thermodynamic data such as enthalpy of formation. Over the last 5 years, a program to experimentally determine enthalpies of formation of Heusler compounds has been undertaken (see for example [9, 10]) and a large dataset now exists [11]. These data are of use in Calphad calculations as well as providing benchmarks for first principles calculations. Furthermore, the Calphad approach cannot predict the occurrence of a particular intermetallic compound, whereas first principles calculations can and it is often necessary to

✉ Philip Nash
nash@iit.edu

[1] Thermal Processing Technology Center, IIT, Chicago, IL 60616, USA

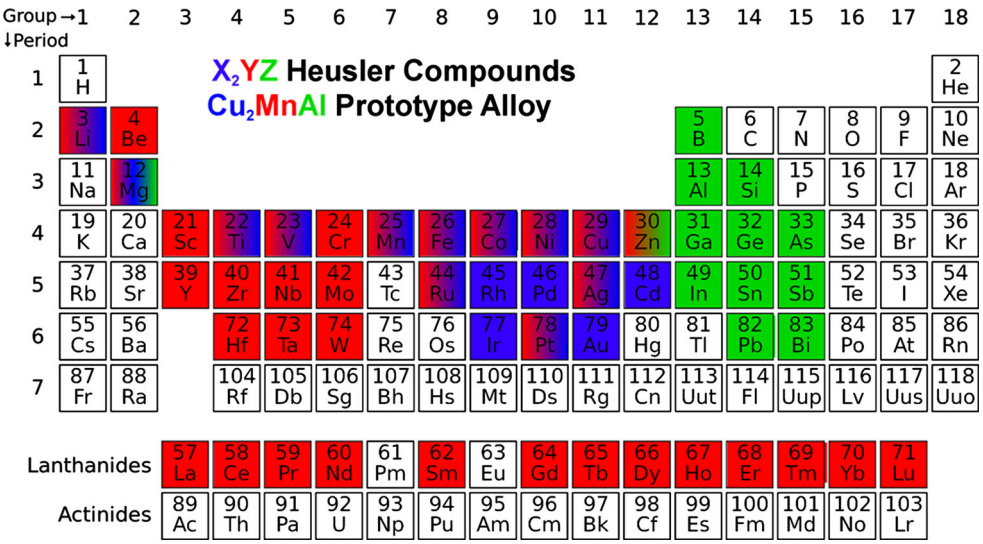

Fig. 1 Periodic table showing typical X, Y and Z elements in Heusler compounds. Modified from blank table image: http://en.wikipedia.org/wiki/File:Periodic_table_%28polyatomic%29.svg Available under CC-BY-SA license: http://creativecommons.org/licenses/by-sa/3.0/deed.en

use a hybrid approach utilizing experiment, Calphad and first principles calculations to provide accurate descriptions of the phase equilibria in complex alloy systems [12].

Given the large number of possible compounds, the use of high throughput first principles calculations to establish stability of a compound provides a useful guide in the search for new Heusler compounds [13–18]. Nevertheless, such calculations sometimes contradict experimental observations, for example, for the compound Ni_2MnSn ($L2_1$) which is predicted to be less stable than corresponding binary compounds; however, the existence of the phase is well established [19–21].

The need for phase equilibria data over a range of temperature is made more apparent by the observation that it is possible for Heusler compounds to form on cooling from either an A2 bcc solid solution phase, or a B2 primitive cubic-ordered phase. Such transformations may occur by first-order or second-order, ordering transformations. This is due to the structural relationship between these phases as shown in Fig. 2. Such transformations may also be valuable for example in processing bulk material which is usually difficult for the highly ordered Heusler compound [22]. Furthermore, some properties require constitutional defect structures introduced by compositions off-stoichiometry [23, 24] or doping of the ternary intermetallic with a fourth element to promote optimum properties, e.g. thermoelectrics [24–26]. Shape memory and magnetic properties can be strongly affected by fourth element substitution [3]. This provides us a vast composition-temperature space to explore for the design and development of Heusler containing-materials.

In this paper we review the current knowledge of phase equilibria in Fe, Co or Ni alloy systems containing, or potentially containing, Heusler phases. In order to keep this review manageable we have confined our discussion to systems containing transition metals and Group III–IV elements. A total of 180 ternary systems have been reviewed. We have not attempted to review the specific properties of Heusler alloys as there are several excellent reviews available on this topic [2, 27–31]. We have tried to identify systematic phase equilibria according to elemental constituents and highlight which systems may offer interesting combinations of phases for functional and structural applications. We have also identified ternary systems where additional phase equilibria work is needed and potential Heusler compounds that have yet to be discovered.

Identification of Heusler structure

The identification of the presence of a Heusler compound by X-ray diffraction can sometimes be difficult due to the similarity of the structure to the A2 (prototype W, Pearson symbol cI2, space group $Im\ \bar{3}m$) and B2 (prototype CsCl, Pearson symbol cP2, space group $Pm\ \bar{3}m$) crystal structures, less than perfect order, constitutional defects and similarities in scattering between the constituent elements. It is apparent from Fig. 2 that there are close relationships between these three crystal structures and also a fourth, $C1_b$ structure (prototype AgAsMg, Pearson symbol cF12, space group $F\ \bar{4}3m$). The related $C1_b$ structure, exhibited by half-Heusler compounds, with stoichiometry XYZ, results from the removal of four X atoms from the $L2_1$ structure. Essentially, the B2 is the result of ordering from the A2 structure, and the $L2_1$ corresponds to an ordering of 8 unit cells of B2 structure in a ternary alloy. This is most easily appreciated by shifting the origin to the X atom at 1/4, 1/4, 1/4, where it can be seen that the unit cell is composed of eight B2 type unit cells, four containing the Y element in

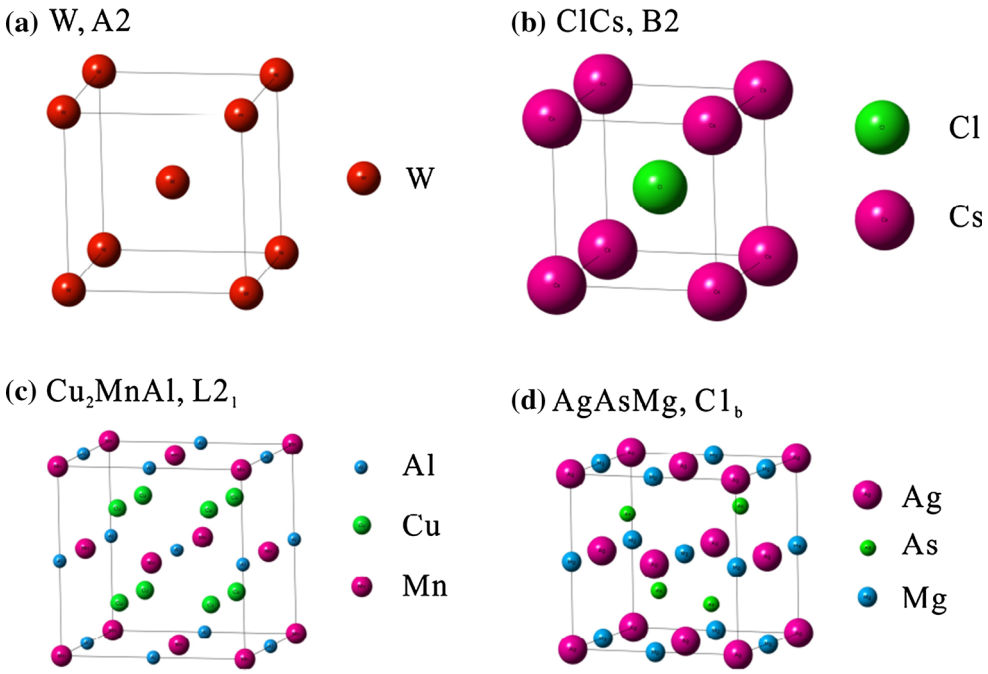

Fig. 2 Unit cells of **a** A2, **b** B2, **c** $L2_1$ and **d** $C1_b$ structures

the central position and four containing the Z element in the central position, Fig. 3c [32]. In a ternary alloy composition X_2YZ with a B2 structure, one of the Wyckoff positions is shared by the Y and Z elements, Fig. 3b. The simulated XRD patterns for $Co_{0.5}Fe_{0.25}Al_{0.25}$ in the 3 different structures are shown in Fig. 4. It is apparent that the major peaks are the same, while additional superlattice peaks appear as the ordering goes to B2 and then to $L2_1$. These simulated patterns are for perfect order and the stoichiometric composition and less intense superlattice lines will occur for non-stoichiometric compositions and lower order. Thus, considerable care must be taken in identifying the Heusler, $L2_1$, structure in an alloy.

Phase equilibria in Fe containing systems

Table 1 provides an overview of the ternary alloy systems in which an iron-based Heusler phase has been experimentally observed and also indicates those systems for which no experimental phase diagram data exist covering the Fe-based Heusler composition. In addition, we have indicated where existing phase diagrams conflict with single composition work elsewhere in the literature.

Examination of Table 1 shows that Al, Ga, Si, Ge and Sn should be favourable to form the Heusler structure with Fe when present in the Z position, whereas no Ge-containing Heusler compounds have ever been reported experimentally. Shifting our focus to the Y element candidates, the early transition elements in Columns 4 and 5 in the Periodic Table show a tendency to form the Heusler compound with Fe. This trend continues in ab initio prediction down Columns 4 and 5 with the exception of Zr which forms no Heusler phase with Fe. This is due to the relative stability of other phases even though the Fe_2ZrZ compounds are predicted to have negative formation energies. In the Fe–Zr–Si system, the presence of a more stable ternary compound $Fe_{16}Zr_6Si_7$ with a composition close to the Heusler prevents the formation of the Heusler compound [13, 33]. Moving along the transition metal series towards the non-metals, we see a strong trend against Heusler formation with Cr, Ni, Co or Cu. The exception is when Z = Mn which forms Heusler compounds with Al and Si.

Table 2 shows the calculated enthalpies of formation (0 K) for the stable Heusler phases or the difference between the energy of formation and the hull energy, for the predicted unstable Heusler phases taken from the Open Quantum Materials Database (OQMD) [13]. The OQMD is a publicly accessible database of density functional theory (DFT) calculated thermodynamic and structural properties. The hull energy is a convex surface representing the minimum energy in the system as a function of composition. Compounds that have a negative formation energy that is above the hull energy are therefore metastable compounds. Comparing with Table 1, we see a similar story to Co and Ni. There is one compound, Fe_2CrSi [34], that has been made experimentally, conflicting with 0 K stability predictions. The compound was formed by annealing epitaxially grown thin films at 773 K. The compound is predicted to be only 7 kJ/mol of atoms above the hull energy at 0 K and its stability could be affected by the non-equilibrium processing. There are several predicted compounds yet to

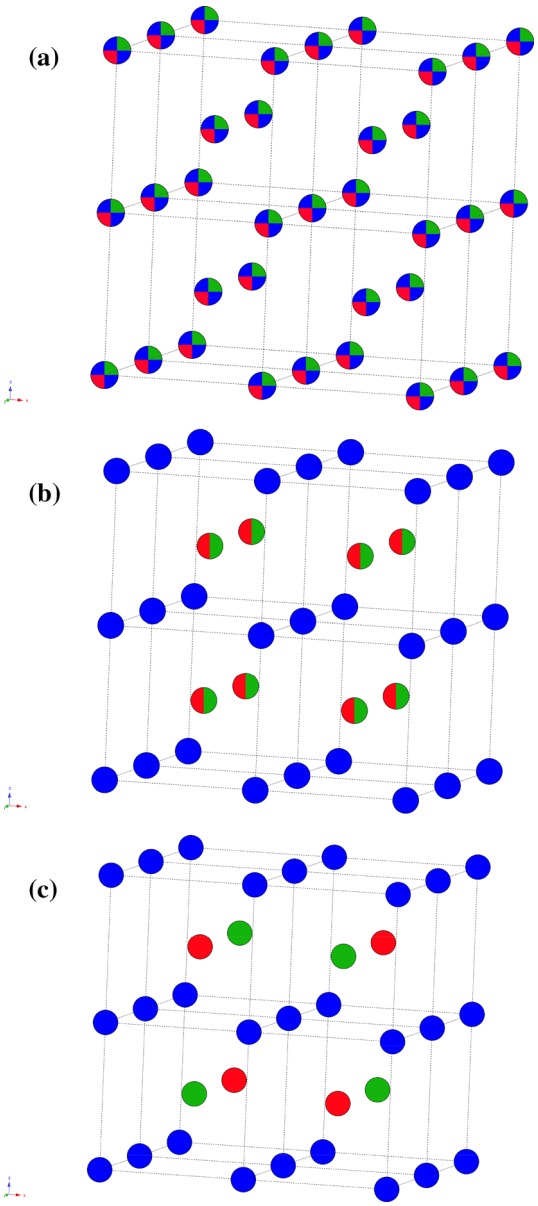

Fig. 3 Co_2FeAl in **a** A2, **b** B2 and **c** $L2_1$ crystal structures. *Blue* atoms represent Co, *red* atoms are Al and *green* atoms are Fe

be verified, and furthermore there are even more cases where the difference between the calculated enthalpy of formation and the hull energy is generally small, less than 5 kJ/mol of atoms, and a Heusler could exist at a non-stoichiometric composition or under non-equilibrium processing. It is worth reiterating that as in the other cases, the calculated hull energy is based on the perfect stoichiometric end members without considering defects or the solubility range, which limits its ability to correctly predict phase stability.

Table 1 hides a number of problems related to the phase equilibria of the Fe–Y–Z ternary systems. For example, the Fe_2TiAl Heusler has been investigated for its thermoelectric properties [35]. However, there exist a myriad of conflicting diagrams some showing Heusler structure up to 1200 °C and others devoid of the structure completely. To illustrate how bad the situation is, Fig. 5 presents a set of 3 isothermal sections at 800 °C. The left most section shows continuous transformation as a function of composition at constant temperature from the A2 (Fe)-structured solid solution phase to an ordered B2 FeAl phase and finally an $L2_1$ Fe_2TiAl structure [36]. The middle diagram has continuous ordering between A2 and B2 phases with no Heusler [37], and the right most diagram presents a 2-phase field separating the broad A2/B2 single-phase region and a narrow range of Heusler compositions [38]. Conflicting sets of equilibrium phase stability such as this make alloy design and bulk processing difficult.

Rounding out the Fe_2TiZ compounds, we have even less phase information. Fe_2TiGa is not reported in any phase diagrams, but has been observed as a compound [39]. Fe_2TiSi is seen only as a metastable extension of the $D0_3$ phase, Fe_3Si [40, 41], but has been used as a distinct phase to improve thermoelectric properties of the FeTiSi half-Heusler [42]. For the compound Fe_2TiSn, the crystal structure is verified to be Heusler [32], but no ternary diagram exists. The half-Heusler is stable [43] giving the potential to build a two-phase thermoelectric with higher figure of merit (zT) due to phonon scattering on the phase boundaries reducing the thermal conductivity.

Fe_2VAl is one of the thermoelectric Heusler compounds [44] with relatively advanced development in the form of a vehicle scale powder-metal processed doped bimetal device having been fabricated and tested [45, 46]. This system is not much better explored than the Fe_2TiAl system with the majority of diagrams showing that no Fe_2VAl phase is present. The best data for working with this alloy are confined to a set of partial isothermal sections at 650, 700 and 750 °C [47]. These diagrams do not mesh well with the other data that are also sparse.

Another thermoelectric that has been subject to alloy work is Fe_2VGa. The large solubility range at 800 °C and wide two-phase field with Fe room temperature structure provide opportunities to create a two-phase material with a more ductile matrix [48]. Due to the lack of higher temperature data, equilibria information makes solution treatment and high temperature forging more guesswork than science at this time.

Fe_2VSi and Fe_2MnAl have been confirmed experimentally [32] with Fe_2VSi, in particular, observed at 300 K with a transformation to the tetragonal structure at 120 K. Fe_2MnSi was similarly reported [49]. None of these compounds appear in any of the experimental ternary diagrams currently available ranging from 1473 to 298 K.

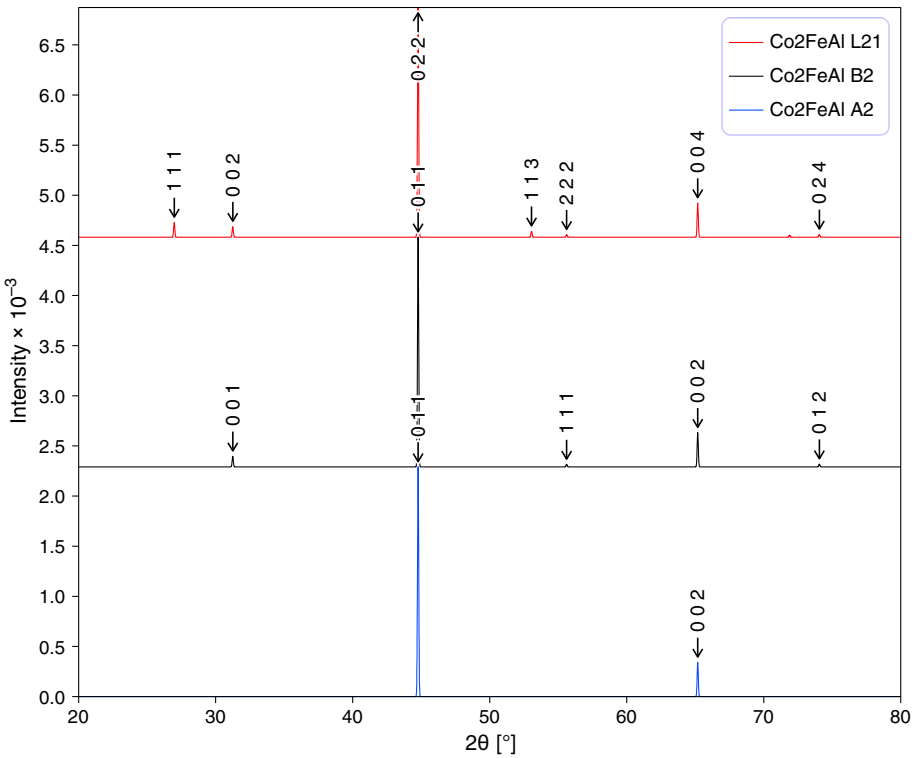

Fig. 4 Calculated XRD patterns for A2, B2 and $L2_1$ structures at the composition Co–25 at.%Fe–25 at.%Al using Cu K_α X-ray wavelength

Fe_2TiGe, Fe_2NbAl, Fe_2NbGa, Fe_2TaAl and Fe_2VGe [13, 15], are all predicted as stable compounds at 0 K, but do not appear in any of the existing phase diagrams nor do they show up in other experimental work. The most unexplored frontier is that of compounds predicted stable ab initio, but for which there are no phase diagrams: Fe_2TaGa, Fe_2TaGe and Fe_2HfSn.

Phase equilibria in Co-containing systems

Table 3 provides an overview of the ternary alloy systems in which a cobalt-based Heusler phase has been experimentally observed and also indicates those systems for which no experimental phase diagram data exist covering the Co-based Heusler composition. Only two of the 11 possible systems with In are reported to have a Heusler phase, Co_2FeIn [32] and Co_2CrIn [50], and no phase diagrams are available for any of these systems. The possibility exists that some of the other systems may also contain an as yet undiscovered Heusler phase. A general observation for the formation of a Heusler phase in Cobalt containing alloys is that no Heusler phase is observed when either Ni or Cu is the Y element. An ordered compound has been reported [51] for Co_2NiGa which was synthesized by mechanical alloying but was not observed in arc-melted samples. However, the ordered compound is reported to have a Pt_2FeCu prototype structure, rather than the Cu_2MnAl structure of Heusler compounds. On the other hand, if the Y element is from the first two columns of the transition metal series, a Heusler phase is observed.

For those systems with no phase equilibria data available, we can make some observations about the likelihood of Heusler phase existence. For the systems Co_2NiZ and Co_2CuZ, we should not expect the presence of a Heusler phase as none have been observed in any of the known phase diagrams and there are no reports of the existence of the $L2_1$ phase in any of these systems. We can also look at predicted stability from first principles calculations. There is a general trend in the Co_2NiZ and Co_2CuZ compositions of a decreasing stability on going down the Group III and IV columns, and the compositions with Z = Sn or In have a positive formation energy at 0 K [13]. For the other Z elements, with small negative energies of formation, they are not predicted to be stable as a result of having energies higher than the hull energy resulting from more stable compounds at other compositions, Table 4. This trend of decreasing stability has been observed experimentally [9].

In systems containing an early transition metal series Y element, many ternary compounds form, for example, 13, 10 and 4, respectively, in the Zr, Hf and Ti containing systems with Ga [52–54]. This results in numerous two- and three-phase equilibria between the Heusler compounds and other phases. This offers the opportunity to combine functional properties of different compounds to produce multifunctional materials. The Co–Hf–Ga system contains 10 ternary compounds many of which have extended

Table 1 The distribution of Fe_2YZ Heusler phases and associated phase diagrams

	Al	Ga	In	Si	Ge	Sn
Ti	Y/H/B	Y/B/η	N	Y/H/B	Y	N/H
V	Y/B/D/H	Y/H	N	Y/B/η	Y	Y
Cr	Y/B	Y	N	Y/B/η	N	N
Mn	Y/B/η	N	N	Y/B/η	Y	Y
Ni	Y/B	Y	N	Y/B	Y	Y
Co	Y/B	N	N	Y/B	Y	Y
Cu	Y/B	N	N	Y/B	Y	Y
Zr	Y/B	Y/B	N	Y/B	N	N
Nb	Y/B	Y	N	Y/B	N	N
Hf	Y/B	Y	N	N	Y	N
Ta	Y/B	N	N	N	N	N

Y or N indicates if a published measured phase diagram is available or not

H indicates that the Heusler phase has been reported experimentally in this system in a phase diagram

B indicates that the B2 phase has been reported experimentally in this system

D indicates that the $D0_3$ phase has been reported experimentally in this system

η indicates that a Heusler has been reported exclusively outside of phase diagrams in the literature

Red indicates predicted Heusler with no experimental confirmation

Green indicates predicted Heusler with experimental confirmation

Magenta indicates compound not predicted at 0 K, but observed experimentally

Table 2 The calculated enthalpy of formation of Fe_2YZ Heusler compounds or the difference between Heusler energy and hull energy if unstable

	Al	Ga	In	Si	Ge	Sn
Ti	-45	-36	15	-68	-48	-29
V	-41	-29	20	-47	-23	9
Cr	3	8	38	7	9	21
Mn	-18	4	51	-33	0	13
Ni	23	18	36	15	14	26
Co	16	13	29	11	11	22
Cu	19	18	30	19	16	23
Zr	4	10	22	12	9	5
Nb	-36	-25	11	9	8	4
Hf	0	6	20	6	4	-27
Ta	-44	-31	12	5	-22	3

Data in kJ/mol of atoms

Italicized values correspond to the calculated enthalpy of formation (0 K) when the Heusler structure is indicated to be stable by the OQMD/AFLOW

Orange values correspond to the difference between enthalpy of formation of the Heusler phase and the hull energy when the Heusler formation energy is greater than the hull energy

solubility at constant Hf content, that is, there is site substitution between Co and Ga. This is also exhibited by some of the binary compounds. Interestingly, the compound Co_2HfGa goes against this trend by having extended solubility at constant Co content indicating Ga substitution for Hf, but not vice versa, that is the phase field does not extend to higher Hf contents than 50 at.%, Fig. 6 [53] Furthermore, this Heusler compound is in equilibrium with the B2 compound CoGa and the compound CoHfGa. In the Co–Ti–Ga system, a small composition range of Co_2TiGa is in equilibrium with a large composition range of CoGa offering the possibility of tuning properties through variation of volume fraction and phase compositions.

In systems with two binary B2 phases containing Co, the possibility exists for complete solid solubility from one to the other. This in turn leads to the possibility of a first or second-order ordering transformation to the $L2_1$ phase since they are structurally related, Fig. 2. An example of this is Co–Fe–Ga [55] which has an extensive $L2_1$ single-phase field covering the compositions Co_2FeGa and Fe_2CoGa as well as B2 phases CoGa and CoFe, Fig. 7. In this system, continuous ordering is observed from B2 to $L2_1$ on

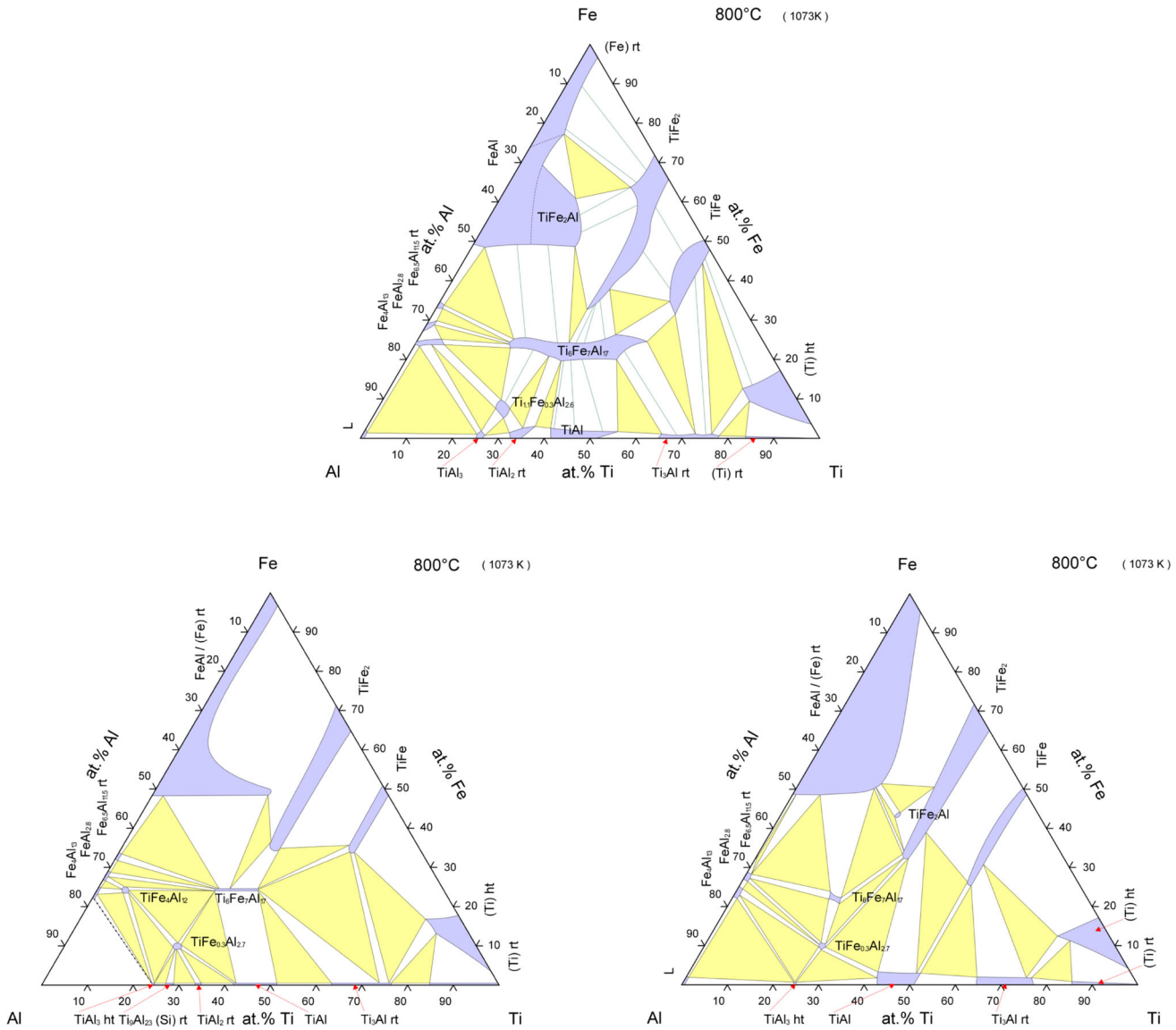

Fig. 5 Three experimentally determined isothermal sections at 1073 K for the Fe–Ti–Al system. Reproduced from [36, 37, 168–171] with permission from Springer

decreasing the temperature. This also occurs in the Co–Cr–Ga [56] and the Co–Mn–Ga [57] systems.

In other cases, the Heusler phase is stable to the melting point and continuous ordering occurs from the B2 phases for off-stoichiometric compositions with phase separation occurring at lower temperatures, for example, Co–Ti–Al, Figs. 8 and 9 [58]. Through suitable choice of composition, it is then possible to have a single-phase structure at high temperature and a two-phase Heusler + B2 structure at low temperature.

The systems Co–Y–Sn with Y = Ti, Zr, Hf exhibit extension of the ternary phase at the composition Co_2YSn along a constant 1:1 ratio of Y:Sn. The Hf-containing compound provides some small solubility extension on either side of the 1:1 ratio. For the Hf- and Zr-containing compounds, there is no equilibrium between the Heusler phase and Co due to the intervention of binary phases. However, for Co_2TiSn, there is an equilibrium with Co and since both phases are magnetic this could provide some interesting magnetic phenomena. Indeed this has been investigated [59] and unusual coercivity versus temperature behaviour was observed. The isothermal section determined by Stadnyk et al. [60] shows that there is a continuous solid solution from the Co_2TiSn (prototype Cu_2MnAl) composition to CoTiSn (prototype MgAgAs). This continuous change in order occurs by substitution of Co atoms by vacancies and gives a change in properties [61], which appears not to have been fully investigated to

Table 3 The distribution of Co_2YZ Heusler phases and associated phase diagrams

	Al	Ga	In	Si	Ge	Sn
Ti	Y/H	Y/H	N	Y/H	N/ η	Y/H
V	N/ η	Y/H	N	Y/H	N	N/ η
Cr	Y/ η	Y/ η	N/ η	Y	N	N
Mn	Y/ η	N/ η	N	Y/H	N/ η	N/ η
Fe	Y/D	N/ η	N/ η	Y/ η	N/D	Y
Ni	Y	Y	N	Y	N	N
Cu	Y	N/D	N	Y	N	N
Zr	Y/H	Y	N	Y	N	Y/H
Nb	Y/H	N/H	N	Y	N	Y/H
Hf	Y/H	Y/H	N	N	Y	Y/H
Ta	N/H	N/H	N	N	N	N

Y or N indicates if a published measured phase diagram is available or not

H indicates that the Heusler phase has been reported experimentally in this system in a phase diagram

B indicates that the B2 phase has been reported experimentally in this system

D indicates that the $D0_3$ phase has been reported experimentally in this system

η indicates that a Heusler has been reported exclusively outside of phase diagrams in the literature

Red indicates predicted Heusler with no experimental confirmation

Green indicates predicted Heusler with experimental confirmation

Magenta indicates compound not predicted at 0 K but observed experimentally

Table 4 The calculated enthalpy of formation of Co_2YZ Heusler compounds or the difference between Heusler energy and hull energy if unstable

	Al	Ga	In	Si	Ge	Sn
Ti	-60	-51	-24	-65	-49	-38
V	-40	-29	14	3	-22	8
Cr	7	3	21	4	0	9
Mn	-35	-22	8	-43	-24	-13
Fe	-35	-22	10	-34	-16	7
Ni	13	10	28	9	7	18
Cu	16	11	25	9	5	12
Zr	-49	-42	-25	16	9	-39
Nb	-40	-30	3	21	12	2
Hf	-55	-47	-28	13	7	-40
Ta	-45	-33	7	20	11	5

Data in kJ/mol of atoms

Italicized values correspond to the calculated enthalpy of formation (0 K) when the Heusler structure is indicated to be stable by the OQMD/AFLOW

Orange values correspond to the difference between enthalpy of formation of the Heusler phase and the hull energy when the Heusler formation energy is greater than the hull energy

date. The properties of the stoichiometric Co_2TiSn have been extensively studied (see for example [62–65]) and show that the compound is a half-metallic ferromagnet. It has a constant Seebeck coefficient as a function of temperature and combined with the half-metallic behaviour this makes the material potentially useful for thermoelectric and spintronic applications [62]. Since there is interest in improving thermoelectric properties through the use of multi-phase alloys [24, 26, 66], the phases in equilibrium with Co_2TiSn are worth noting. Unfortunately, there are discrepancies between the available isothermal sections at different temperatures 1070 K [60] and 870 and 1070 K [67]. The results by Yin et al. [67] are based on CALPHAD modelling and indicate a two-phase equilibrium between Co_2TiSn and CoTiSn. However, the experimental work by Stadnyk et al. [60] indicates a continuous phase field from Co_2TiSn to CoTiSn and we will assume for the purposes of discussion that this is correct. Because of the extended

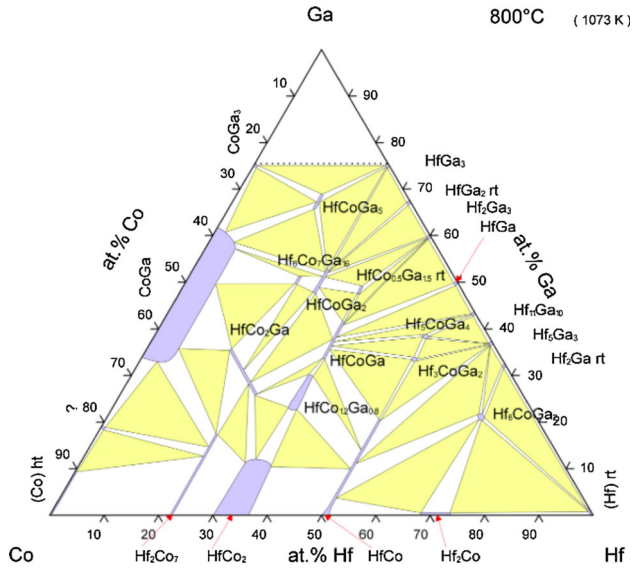

Fig. 6 The Co–Hf–Ga 1073 K isothermal section. Reproduced from [177, 178] with permission from Springer

solubility of the Co_2TiSn/CoTiSn phase at constant Ti:Sn ratio, the phase equilibria involve many different binary compounds in the Co–Ti and Co–Sn systems. There is also a two-phase equilibrium with the Co solid solution that has almost no solubility for the Sn but up to 10 at.% for Ti. The two-phase fields are quite narrow so the isothermal section at 1070 K is dominated by a large number of three-phase fields [60]. The Co–Zr–Sn is very similar to Co–Ti–Sn except that the Co_2ZrSn phase does not extend all the way to CoZrSn and there is a two-phase equilibrium between the two phases at 770 K.

The systems Co–Fe–Z offer some interesting possibilities for phase equilibria involving order–disorder transformations. Also there could be equilibria between Heusler phases and ductile phases that offer the potential of bulk processing. In the Co–Fe–Al system, there are substantial solid solution regions for different phases. Both B2 and $L2_1$ structures have been reported at the stoichiometric composition Co_2FeAl [68–71]. Balke et al. claimed that Co_2FeAl crystallizes in the B2 structure based on an annealing treatment of their arc-melted samples at 1300 K [70]. The variation in reported structure suggests that the Heusler phase may result from an ordering of the B2 on cooling below 1300 K. This is not shown on any published isothermal section, even one calculated for 600 K [72], and a review of the phase equilibria in this system concludes that there are no ternary compounds [73]. An experimental section determined at 923 K only shows the B2 phase present at the Co_2FeAl composition [74, 75]. The phase diagram as a function of composition along a 50 at.% Co

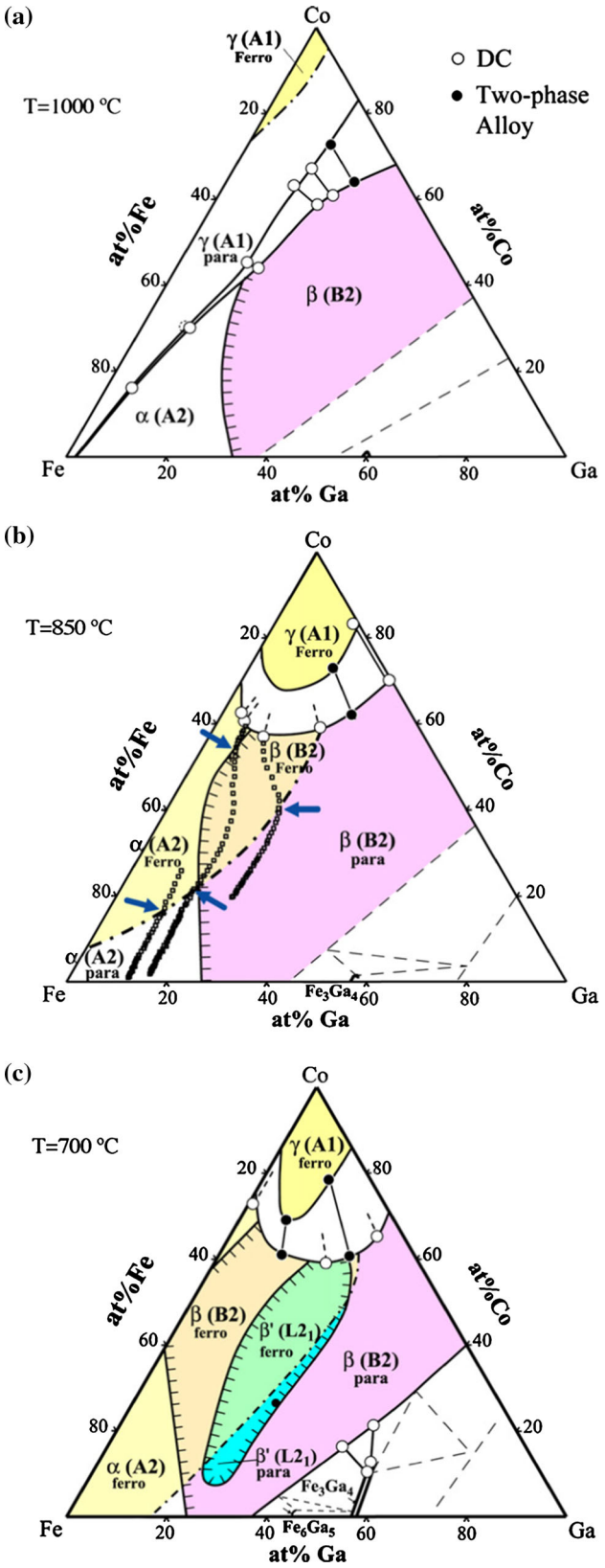

Fig. 7 Co–Fe–Ga isothermal sections. Reproduced from [55] with permission from Elsevier

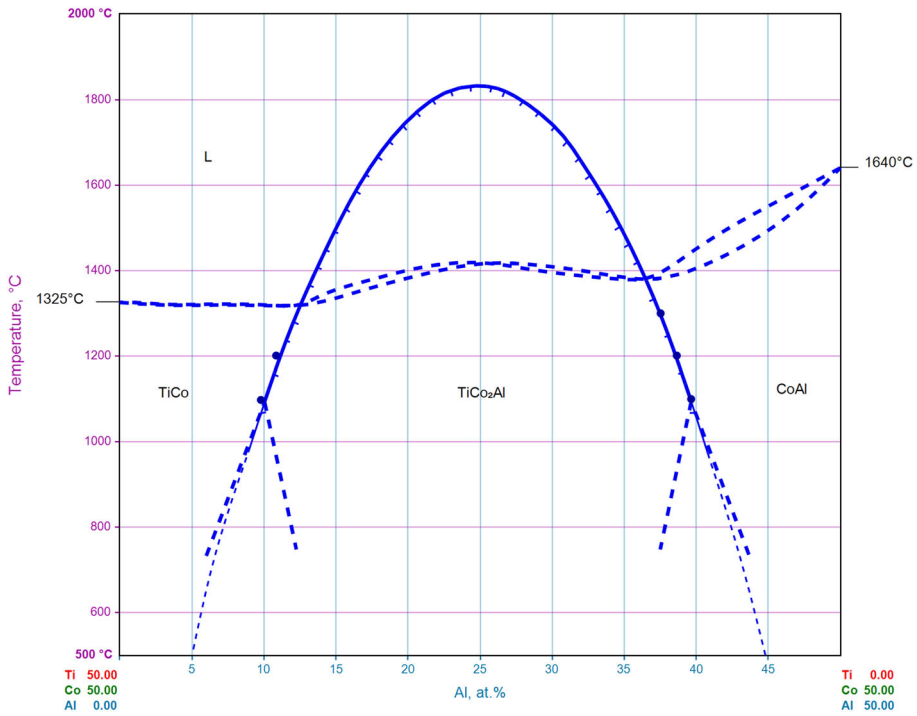

Fig. 8 Pseudobinary section CoTi–CoAl showing metastable extension of the Co_2TiAl phase field [58]. Reproduced from [172] with permission from Springer and MSIT® MSI Eureka

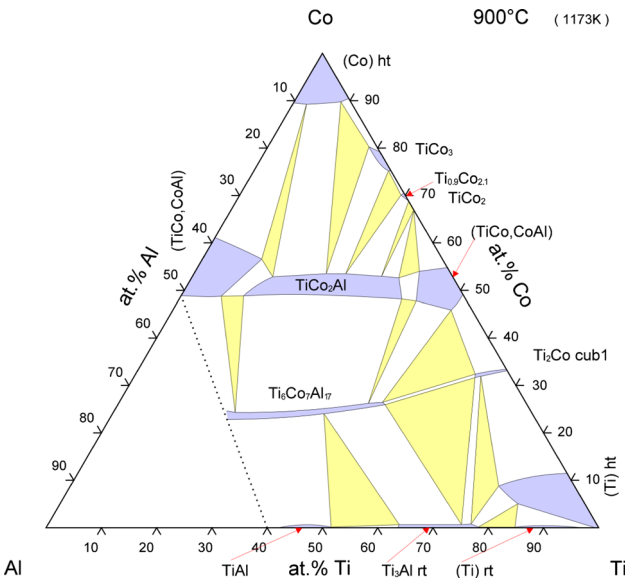

Fig. 9 Isothermal section Co–Ti–Al at 1173 K. Reproduced from [173, 174] with permission from Springer

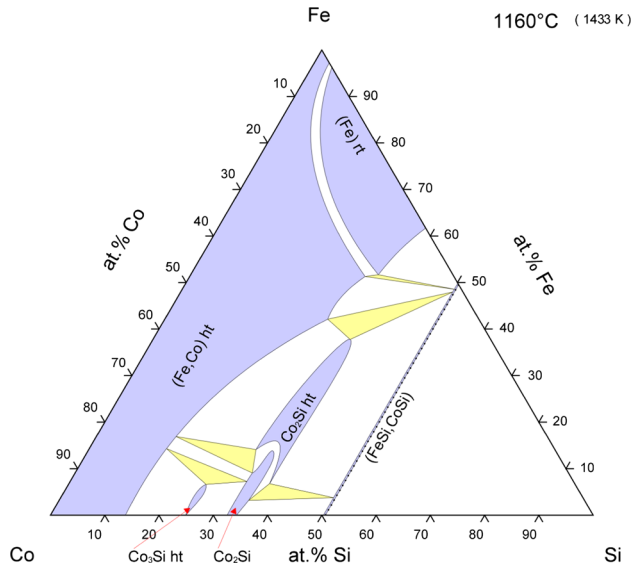

Fig. 10 Co–Fe–Si isothermal section at 1433 K. Reproduced from [175, 176] with permission from Springer

isopleth was investigated by Kogachi [69] who showed there was a second-order order/disorder transition $B2/L2_1$ with a maximum temperature at about 973 K, with the Heusler phase existing over a range of composition from 19 at.% Fe to 35 at.% Fe. Due to less than perfect order in the $L2_1$ phase, it was difficult to determine the limits of the transition. Later work by Balke et al. [5] on $Co_2FeAl_{1-x}Si_x$ shows an $A2 + B2$ to $B2 + L2_1$ order transition at a temperature of 1190 K for the Co_2FeAl composition. This is not consistent with the work by Kogachi [69] and it would be of value to reinvestigate the phase equilibria over a range of compositions to define the composition range of the $L2_1$ phase field. As can be seen in Fig. 4, ordering from A2 to B2 and then to $L2_1$ results in additional diffraction lines (superlattice lines) with relatively weak intensity, making identification of the $L2_1$ ordering difficult as the transition temperature is approached and the degree of long range order decreases. The $L2_1$ phase is predicted as stable

from ab initio calculations and is predicted to have a substantial formation enthalpy at 0 K of −34.5 kJ/mol [13]. Thus, a reinvestigation of the phase equilibria in the Co–Fe–Al system is needed. No Heusler phase has been reported in either the Co–Fe–In or the Co–Fe–Sn systems. This is consistent with the decreasing stability trend observed on going down the Group III and IV columns [9, 13].

A large number of papers have been published studying the Heusler compound Co_2FeSi, covering thin film and bulk synthesis as well as ab initio studies, see for example [41, 71, 76–84]. The consensus of these reports is that Co_2FeSi exists as an $L2_1$-structured compound to high temperature, if not to the melting point. Partial substitution of Si by Al has been shown to disorder the compound to a B2 structure [82]. It is well established that this compound is a half-metallic ferromagnet (HMF) with a high Curie temperature of 1100 K [81, 85], and is of great interest for application as a spintronic material. The effects on the properties of quaternary additions have been investigated [86] as have the effect of disordering to the B2 phase [87]. It is predicted to be a stable phase in the Co–Fe–Si system by ab initio calculations, and the calculated formation energy of −34 kJ/mol (0 K) [88] compares well with the experimentally measured value of −38.4 kJ/mol (298 K). [9] The melting point for this composition has been measured as 1513 and 1510 K, respectively [89, 90], and both researchers determined a heat effect at 1031 K [89] and 1039 K [90] interpreted as a B2 ⇒ $L2_1$ order transformation. However, Wurmehl et al. [85] annealed Co_2FeSi arc-melted samples at 1300 K for 20 days and obtained the $L2_1$ structure. Shreder et al. [71] melted alloys and obtained the $L2_1$ structure without further annealing. These results are insufficient to adequately understand the ordering behaviour in this material and this warrants further investigation. In many papers, the details of the preparation of the Co_2FeSi do not involve determining the state of order and yet it is known that this can vary with preparation technique [41]. Surprisingly, despite the large body of work indicating the existence of the $L2_1$, Co_2FeSi phase, the published phase diagrams [91, [92] do not show the presence of this phase on isothermal sections at 1073 and 1433 K, Fig. 10. This significant discrepancy along with uncertainty regarding a B2-$L2_1$ transition requires a thorough re-evaluation of the phase equilibria in this system.

In the Co–Fe–Sn system, an isothermal section at 298 K is available [93], which does not show the presence of a Heusler phase. Furthermore, experimental work on bulk alloys has not shown the existence of the Heusler phase [9, 94], although it was found to be stable in quaternary alloys $Co_2Mn_{1-x}Fe_xSn$ when x was less than 0.5 [95]. Li et al. [96] and Duan et al. [97] reported synthesizing B2 structured nanoparticles of Co_2FeSn by an electrodeposition method and a solution reduction method. However, the Heusler phase was reported by Tanaka et al. [98] based on the production of thin films by an atomically controlled alternate deposition process. Further work also indicates the existence of the $L2_1$ phase after non-equilibrium processing [99]. The Heusler phase is predicted from ab initio calculations to have a negative formation energy of −2.8 kJ/mol, but not to be stable relative to other phases by +7.3 kJ/mol [13]. The relatively small energy difference may allow the formation of the Heusler phase through non-equilibrium processing as demonstrated by Tanaka et al. [98]. Based on this observation, we have identified in Table 4 a number of other Heusler compounds that also have negative formation energies and small energy differences above the hull energy, as these may also yield a Heusler phase on non-equilibrium processing.

In the Co_2MnZ compounds, half metallicity has been shown for compounds with Z = Al, Ga, Sn, Si and Ge [4]. The crystal structure, electronic structure and magnetic properties of quaternary Heusler compounds of the type $Co_{2-x}Rh_xMnZ$ (Z = Ga, Sn, Sb) have been investigated and it was noted that the quaternary addition led to different types of anti-site disorder [100]. The compound Co_2MnIn is not predicted to be stable, Table 4, nor have a negative energy of formation at 0 K according to ab initio calculations. However, the existence of the Heusler phase has been reported in annealed, melt spun ribbons of $Co_{50}Mn_{30}In_{20}$ [101]. The phase equilibria in the Co–Mn–Ga system have recently been investigated [57]. Isothermal sections at 1000, 900 and 800 °C were determined experimentally as well as the B2/$L2_1$ ordering temperature and $L2_1$ Curie temperature along the 50 at.% Co isopleth. The B2/$L2_1$ ordering temperature shows a maximum around 900 °C at the stoichiometric Heusler composition, Co_2MnGa.

Comparing ab initio calculations of stability at 0 K, Table 4, with the information in Table 3, we can see that two other compounds that are known to have Heusler phases, Co_2CrIn [50] and Co_2VSi [9, 49, 102] are not predicted to be stable, although Co_2VSi does have a substantial energy of formation, −40.9 kJ/mol and the energy difference above the hull energy is small, +2.9 kJ/mol. On the other hand, the ab initio calculations predict stable Heusler phases for a number of potential compounds that have not yet been reported and in most cases the alloy systems do not have a phase diagram. The compounds are Co_2ZrGa, Co_2ZrIn, Co_2TiIn, Co_2HfIn and Co_2VGe. These should be investigated as potentially new Heusler phases can be discovered. The Co–Zr–Ga system is predicted to have a stable Heusler phase but an isothermal section at 1073 K shows a different phase, $Co_{11}Zr_4Ga_5$ at about the Heusler phase composition [52]. This system is therefore a good candidate for some reinvestigation around the Heusler composition.

Table 5 The distribution of Ni_2YZ Heusler phases and associated phase diagrams

	Al	Ga	In	Si	Ge	Sn
Ti	Y/H	Y/H	Y/H	Y	N	Y/H
V	Y/B	Y/H	N	Y	N	N/η
Cr	Y/H	Y	N	Y	N	N
Mn	Y/H	N/η	Y/H	Y	N/η	N/ η
Fe	Y/H	Y/H	N	Y	N	Y
Co	Y	Y/B	N	Y	N	N
Cu	Y	N	N	Y	Y	Y/D
Zr	Y/H	Y/H	N/H	Y	N	Y/H
Nb	Y/H	N/ η	N	Y	N	Y/H
Hf	Y/H	Y/H	Y/H	N	N	Y/H
Ta	Y/H	N/ η	N	N	N	N

Y or N indicates if a published measured phase diagram is available or not

H indicates the Heusler phase has been reported experimentally in this system in a phase diagram

B indicates the B2 phase has been reported experimentally in this system

D indicates the $D0_3$ phase has been reported experimentally in this system

η indicates that a Heusler has been reported exclusively outside of phase diagrams in the literature

Red indicates predicted Heusler with no experimental confirmation

Green indicates predicted Heusler with experimental confirmation

Magenta indicates compound not predicted at 0 K but observed experimentally

Table 6 The calculated enthalpy of formation of Ni_2YZ Heusler compounds or the difference between Heusler energy and hull energy if unstable

	Al	Ga	In	Si	Ge	Sn
Ti	-61	-53	2	9	5	3
V	5	2	15	12	10	11
Cr	12	11	14	18	13	12
Mn	-40	0	3	5	1	0
Fe	7	5	12	12	9	11
Co	16	13	20	17	15	17
Cu	2	1	4	7	3	3
Zr	-59	11	-41	18	11	-52
Nb	0	0	3	25	15	4
Hf	-62	0	0	17	10	-51
Ta	1	0	7	24	17	9

Data in kJ/mol of atoms

Italicized values correspond to the calculated enthalpy of formation (0 K), when the Heusler structure is indicated to be stable by the OQMD/AFLOW

Orange values correspond to the difference between enthalpy of formation of the Heusler phase and the hull energy when the Heusler formation energy is greater than the hull energy

The Co–Y–Z systems with Y = V, Nb, Ta and Z a group III–IV element exhibit a number of ternary compounds. The Co–Nb–Al system has received extensive experimental study and has been the subject of a recent Calphad type modelling [103–105]. Isothermal sections are available at 4 different temperatures [103], as well as a liquidus projection [104] and with the Calphad model this system represents a good example of the extent of phase equilibria needed for alloy development. In this system, the Heusler phase Co_2NbAl [106] is in equilibrium over a large range of composition with CoNbAl which is an hexagonal Laves phase, prototype $MgZn_2$, Pearson symbol C14, space group $P6_3/mmc$ [103, 107]. Furthermore, the isothermal sections show that the Co_2NbAl phase field shrinks with decreasing temperature on the Aluminium-rich side, offering the possibility of precipitation of CoAl in a matrix of the Heusler phase. The Heusler phase is not in equilibrium with the (Co) terminal solid solution. In the Co–Nb–Sn system, the single isothermal section available also shows no equilibrium between Co_2NbSn and Co [108]. However, there is an equilibrium between the Heusler and half-Heusler phase, CoNbSn. The Co–V–Si isothermal

section at 1373 K shows the Co_2VSi phase to exist off of the stoichiometric composition [109] and it is in equilibrium with the (Co) terminal solid solution. According to ab initio calculations, the Co_2VSi phase has a negative formation energy but is not predicted to be the stable phase at this composition, being +2.9 kJ/mol above the hull energy formed from CoVSi + Co_3V + Co_2Si. This is not found to be the case in the experimental isothermal section due to the presence of some additional ternary compounds not considered in the ab initio calculations and the experimental equilibrium at this composition is Co_2VSi + $Co_{0.56}V_{0.3}Si_{0.14}$ + $Co_{0.3}V_{0.5}Si_{0.2}$. Co_2VGa exhibits a large solubility region in equilibrium with (Co) and CoGa at 1073 K. The published phase diagram violates Schreinemaker's rule at the Co_2VGa vertex of the Co_2VGa + Co_3V + $Co_{0.4}V_{0.6}$ 3 phase region. No phase diagrams are available for Co–Ta–Z, except for Co–Ta–Al [110] but that is incomplete and does not cover the Heusler composition. However, the Heusler compound Co_2TaAl [106] has been reported in arc-melted samples annealed 24 h at 1173 K and subsequently 72 h at 1073 K. The Heusler compound Co_2TaGa has also been reported [111], but no phase diagram exists.

Phase equilibria in Ni containing systems

Table 5 provides an overview of the ternary alloy systems in which a nickel-based Heusler phase has been experimentally observed and also indicates those systems for which no experimental phase diagram data exist covering the Ni-based Heusler composition.

Examination of Table 5 shows that Al, Ga, In and Sn are favourable to form the Heusler structure with Ni, while no Si- and Ge-containing Heusler compound has ever been reported experimentally so far except for Ni_2MnGe [112, 113]. An Ni_2MnGe film with an $L2_1$ structure was reported by Lee et al. [113] through flash evaporation of crushed alloy powders from arc melting. Marazza et al. [114] prepared Ni_2MnGe Heusler structured alloy using induction melting followed by annealing at 773 K for 15 days but did not provide detailed characterization, and Cherkashin et al. [115] also reported an $L2_1$ structure in Ni_2MnGe but they admitted to having an inhomogeneous sample and the observed Heusler peaks could correspond to the generally observed ternary compound $Ni_{16}Mn_6Ge_7$ (prototype $Cu_{16}Mg_6Si_7$, Pearson symbol cF112, space group $Fm\bar{3}m$) [116]. The first principles calculations by Zayak et al. [117] indicate that Ni_2MnGe with an $L2_1$ structure is unfavourable due to incommensurate phonon instability. The OQMD database predicts that neither the Ni_2MnGe nor the $Ni_{16}Mn_6Ge_7$ phase is stable, even though they have negative formation energies, rather the stable equilibria should be Mn + NiMnGe + Ni_3Ge [13]. The inconsistent results and lack of phase diagram for this system calls for further work to be performed to establish the phase equilibria in this system. As for the Y element, the early transition elements in Columns 4 and 5 in the Periodic Table have a tendency to form the Heusler compound with Ni, while Cr in Column 6 does not. The only reported Heusler compound that contains Cr is Ni_2CrAl [118], although this is not shown in the existing Ni–Cr–Al ternary phase diagrams at 1423 or 1473 K [119, 120], which present a B2 and bcc solid solution two-phase region. More detailed work is needed to resolve the contradiction. The refractory elements, Nb and Ta, form the Heusler structure with Al or Ga as the Z element. Ni_2MnZ has four assured Heusler compounds out of the six possible members, while the late transition elements Fe, Co and Cu do not form the stable Heusler structure with Ni easily. The reported Heusler structure of this type is Ni_2FeAl from melt-spinning technique [121], Ni_2FeGa [122, 123] and a B2 phase found in Ni_2CoGa [124] alloys, while a $D0_3$ structure is observed in the Ni_2CuSn [125] alloy. It should be noted that the equilibrium Al–Fe–Ni phase diagram evaluated by Zhang et al. [121] indicates a B2 structure at the $Ni_{50}Fe_{25}Al_{25}$ composition.

The calculated enthalpies of formation (0 K) for the stable Heusler phases or the difference between the enthalpy of formation and the hull energy for the predicted unstable Heusler phases in the OQMD are compiled in Table 6. Comparing with Table 5, it is obvious that many predicted unstable Heusler phases have been verified to be stable experimentally, such as Ni_2MnIn and Ni_2TiSn. But it should be pointed out that in these cases, the difference between the calculated enthalpy of formation and the hull energy is generally small, less than 5 kJ/mol of atoms. While for Heusler compositions without experimental verification, the difference is often larger than 10 kJ/mol of atoms, such as "Ni_2FeSn" and "Ni_2VIn". It is worth noting that the calculated hull energy is based on the perfect stoichiometric end members without considering defects or the solubility range, which could be the limitation of its ability for predicting the phase stability.

Similar to the Co-containing systems, those with early transition metals (Ti, Zr, Hf) tend to have multiple binary and ternary compounds with limited solid solubility, e.g. Ni–Zr–Ga, Ni–Zr–Al systems and the Ni–Ti–Sn system, shown as an example in Fig. 11. This is quite easy to understand considering the great difference of electronegativity of the early transition metals with the other constitutional elements. It also explains the existence of the half-Heusler compounds in these systems that contain Sn since the half-Heusler structure is favoured when the chemical bond in between is to some extent covalent to make the structure that is composed of 25 % vacancies stable. While in regards of the systems that contain Al and

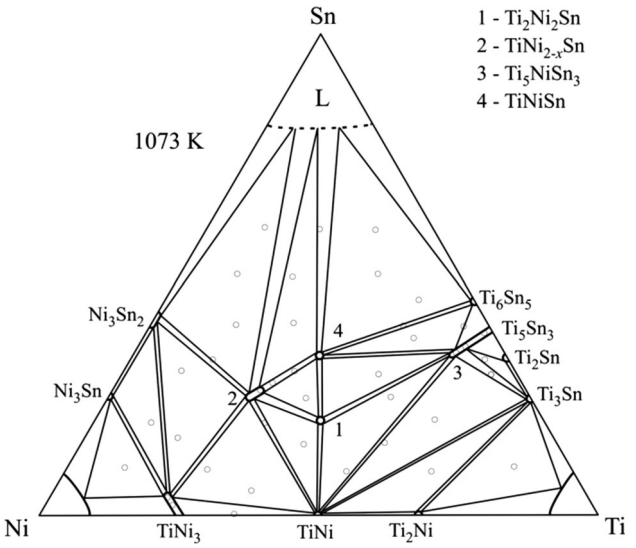

Fig. 11 Isothermal section of Ni–Ti–Sn at 770 K. The circles represent the alloy compositions used to experimentally determine this section. Reproduced from [179] with permission from Elsevier

Ga, the equiatomic composition prefers to form a hexagonal structure (prototype AlNiZr, Pearson symbol hP9, space group $P\bar{6}2m$). For systems where the Z element is Si or Ge, an orthorhombic structure (prototype NiSiTi, Pearson symbol oP12, space group *Pnma*) is observed at the equiatomic composition.

Half-Heusler compounds are of considerable interest as non-toxic candidates for thermoelectric application and are observed in the NiYSn systems (Y = Ti, Zr, Hf) forming an equilibrium triangle with the Heusler compound Ni_2YSn and Ni_3Sn_2 (ht) with almost no solubility range even at a relatively high temperature (around 1000 K) [126–128]. The equilibrium between liquid phase Sn and the half-Heusler phase calls for special attention when preparing the half-Heusler phase to avoid grain boundary weakness. It is worth mentioning that phase separation through introducing a fourth element such as Zr or Hf will further improve their thermoelectric properties through reducing the lattice thermal conductivity due to the solid solution effect [129] and boundary scattering from the nanoscale phase separation [130]. Through solid-state reaction of pre-synthesized half-Heusler alloy with elemental Ni followed by spark plasma sintering, Makongo et al. [131] prepared bulk (Zr, Hf, Ti) NiSn half-Heusler composites containing nanoscale full-Heusler inclusions, showing an increase of electronic conductivity and moderate decrease of thermal conductivity, leading to a drastic improvement of the figure of merit. Furthermore, it is possible to tune the thermodynamic properties such as standard enthalpy of formation and lattice parameters to satisfy certain requirements without degrading other properties.

Ni–Ti–Z systems are especially attractive considering the simultaneous presence of two possible shape memory phases in the same system, the Heusler phase Ni_2TiZ and NiTi. Special interest is devoted to Ni–Ti–Z (Z = Al, Ga) due to the equilibrium between the B2 phase NiZ and the Heusler phase Ni_2TiZ, since after proper selection of alloy composition, the Heusler phase could coherently precipitate out as the strengthening phase [132–134]. The creep strength of the structural alloy NiAl can also be enhanced to a remarkable degree arising from the high-intrinsic creep strength of the non-stoichiometric B2 and $L2_1$ phase [135]. However, the equilibrium between Ni_2TiAl and NiTi is disrupted at a higher temperature of 1400 K [136] by the liquid phase. Therefore, the temperature for heat treatment should be chosen carefully.

Yield strength of Ni–Hf–Al alloys increases with the increasing percentage of Heusler phase Ni_2HfAl (15–96 %) [137], but it was found that precipitation of Ni_2HfAl in a NiAl–0.5–1 at.% Hf alloy was detrimental to the creep properties [138, 139]. Later work established that the precipitation of Ni_2HfAl in NiAl-based alloys is heterogeneous and controlled by the interfacial energy term [140]. It is reasonable to expect that Ni_2NbAl and Ni_2TaAl precipitates can serve in a strengthening function in Ni-based superalloys for turbine blade applications. Limited solubility range is observed in these cases [141, 142], even at high temperature. It is desirable to have isothermal sections at different temperatures or isopleths established so that the amount of precipitate could be controlled quantitatively.

Ni–Mn–Z alloys were investigated extensively due to the special magnetic properties introduced by the unique configuration of the Mn *d*-orbitals [143–145]. New properties with wide potential applications can be obtained through combining the ferromagnetic property and other properties, such as the magneto-optical effect, giant magneto-resistance and magneto-caloric effect. One that draws the most attention is the magnetic shape memory effect in the off-stoichiometric composition in the Ni–Mn–Z alloys. Relatively high Curie temperature and a high efficiency of magneto-mechanical transformation make them very promising for applications as actuators, sensors and for the recording and storage of information. Substantial research has been devoted to further improve the performance. Rapid solidification using advanced synthesizing methods such as melt spinning helps avoid severe compositional inhomogeneity and the resulting metastable nanoscale or even amorphous phase can impart ductility to the brittle Heusler phase [146]. Additionally, the Curie temperature of Ni_2MnSn can be tuned with the substitution of Ni at the Mn sites without a significant reduction in the magnetic entropy change [147].

In the high-temperature (1373 K) isothermal section of Ni–Mn–Al system [148], B2 phase covers more than half of the composition triangle, providing a huge space to explore and design alloys. Again, the phase equilibrium between the Heusler phase and $L1_2$, Ni_3Al and Ni solid solution makes it possible to function as the strengthening precipitate phase. Recently, precipita tion of nanoscale Ni_2MnAl has been designed into an Fe–Mn maraging steel to obtain significant strengthening effect [149]. It is interesting to note that in the Ni–Mn–In ternary system [150], Mn and In tend to substitute for each other very well, even better than Ni–Mn. Continuous increase of the off-stoichiometric composition will change the ferromagnetic alloy into paramagnetic. Even though very little experimental phase diagram information is currently available on Ni–Mn–Ga nor Ni–Mn–Sn systems, it is assured that a wide solubility range will be observed since a large number of off-stoichiometric alloys have been prepared successfully [151–156]. The effect of variations from the stoichiometric composition was investigated theoretically using first principles calculations [157–159]. The results indicate that the stoichiometric composition has the lowest formation energy and that anti-site defects are the favoured constitutional defect. It is reasonable to assume that the Ni_2MnGa Heusler phase would go through order–disorder and merge with the B2 phases NiMn and NiGa, resembling those of Ni–Mn–Al and Ni–Mn–In.

Shape memory alloys Ni–Co–Ga [160] and Ni–Fe–Ga [122] have complete solid solubility from NiGa to CoGa and FeGa due to the similarity between Fe, Co and Ni. Also, there is a larger extent for Fe, Co, Ni to replace Ga than vice versa especially on the Co or Fe side. The off-stoichiometric $L2_1$ Heusler phase $Ni_{0–47}Fe_{75–27}Ga_{27–30}$ was reported at temperatures below 1000 K and the B2 phase disorders and forms the A2 phase in the Fe-rich region. The martensitic phase region determined using the diffusion couple method is located in a wide composition range with 30–40 at.% Ga and 0–50 at.% of Co in the Ni–Co–Ga system and with 30–36 at.% Ga and 0–20 at.% of Fe in the Ni–Fe–Ga system, making them excellent high-temperature magnetic shape memory alloys. While for the Al analogues, less solubility range is observed with regard to the substitution between Al and Fe, Co and Ni. Significant improvement of the ductility can be achieved through introducing fcc Ni solid solution on the grain boundary [161, 162], which requires high-quality phase equilibria and phase transformation information.

Cu and Ni have a complete solubility range and the high-temperature compound Cu_3Sn with a $D0_3$ structure (prototype BiF_3, Pearson symbol cF16, space group *Fm*-3*m*) which is a less ordered form of the $L2_1$ Heusler structure, extends to the $Ni_{25}Cu_{50}Sn_{25}$ composition and even to $Ni_{50}Cu_{25}Sn_{25}$ at 973 K [125]. The Ni-based Heusler structure is predicted to be less stable than the hull energy [13] but does have a negative formation energy of −16.8 kJ/mol [13] or −14.2 kJ/mol [15]. The observed $D0_3$ structure does not order to $L2_1$ at lower temperature instead the stable phase is Cu_3Sn as shown on an isotherm at 513 K [125].

Discussion

The goal of this review is to obtain an overview of the status of knowledge of phase equilibria for a selected group of alloy systems containing or potentially containing a Heusler compound. Experimental work on the ternary phase diagrams is somewhat limited and in some cases non-existent. It is therefore appropriate that we use thermodynamic and ab initio databases to provide guidance in selection of alloy systems and compositions that ultimately require the synthesis of alloys. A database is only as good as the quality of its contents, and such contents are sparse at best and contradictory at worst. If we are to reap, the benefits of computational materials design and materials genome work the source data at the foundation of that work must be robust. Given the promise of multifunctional Heusler materials, there is a need for high-quality phase equilibria data obtained either through experimentation or through the use of reliable computational tools. The absence of such data leaves alloy design work as more art than science, and continued progress reliant on serendipity. Most publications in this field are aimed at determining the properties of a single-alloy composition or in some cases a range of composition for a single compound at a single annealing temperature. Very few publications take a holistic approach of examining the phase relationships to the Heusler phase and the variations in equilibrium with temperature. Needless to say, such studies are time consuming if they rely solely on experimental techniques of phase diagram determination. The combination of microstructural characterization, thermodynamic measurements, thermodynamic computation and first principles calculations of phase stability can provide an efficient method to determine the phase diagram data needed for materials design.

In many instances, where a Heusler compound is reported a single annealing temperature was used, and in some cases arc-melted ingots were used directly. Experience shows that the processing path is important in developing the phase structure and so there is little information regarding the state of a particular composition over a range of temperature outside of the phase diagrams. Furthermore, since the Heusler phase is an ordered intermetallic compound, the state of order and precise composition relative to stoichiometry can affect both the stability

of the phase and its properties. Investigators reporting work on Heusler compounds should be encouraged to determine and report the state of order and actual composition of their material. It can be expected that, for cases where the compound has a negative heat of formation which is only slightly above the hull energy, it may be possible to synthesize the metastable state by some non-equilibrium processing route such as rapid solidification or mechanical alloying.

In the case of thermoelectric materials optimization, modern alloy design is essential in taking a promising compound and transforming it into an efficient device. Heusler and half-Heusler compounds are of great interest due to their high Seebeck coefficients. This ability to generate a large potential difference over a temperature gradient is just one part of the thermoelectric problem. Creating an efficient thermoelectric device requires maximizing the dimensionless figure of merit:

$$zT = (\alpha^2)\sigma T/\kappa,$$

where α is the Seebeck coefficient, σ is the electrical conductivity, κ is the thermal conductivity and T is the temperature. A figure of merit above 1.5 would enable sufficiently efficient generation so as to compete with conventional technologies [163]. Comparable zT have been reported, but to date, production of actual devices has not realized such efficiencies [163]. To push materials beyond the current state of the art necessitates producing a high Seebeck material with high electrical conductivity and low thermal conductivity [163].

Creating divergent conductivities relies on decreasing the lattice contribution to the thermal conductivity. In order to do this, phonon scattering sites must be created on multiple length scales through the creation of phase boundaries, mixed microstructures, refined grains, nanoscale precipitates and point defects [164]. Modern alloy design necessary to obtain each of these features is predicated upon high-fidelity thermodynamic information. Furthermore, reality complicates things with real devices having to operate under conditions dictated by the thermal environment in which it is placed. As such it is not enough simply to maximize zT, but one must tune the peak temperature to the service conditions via alloying [163]. Realizing high efficiency in a real device places an even greater demand for this phase information.

The properties of half-Heusler compounds are also of interest and because of the close relationship with the Heusler phase, these compounds are frequently in equilibrium with each other and in some cases there is a single continuous solid solution from one to the other. This offers the possibility to finely adjust the defect concentration for property optimization. It is also possible to use the two-phase equilibria to advantage in thermoelectric applications where the presence of the Heusler phase improves the thermoelectric properties of the half-Heusler phase [165]. In other cases, the formation of a Heusler/half-Heusler structure can occur by a spinodal decomposition mechanism [131] and such structures offer another design option for the improvement of thermoelectric properties.

On a broader level, microstructural control and a robust knowledge of phase stability and transformation can enable the creation of larger devices in a wider variety of geometries. Conventional forging and heat treatment practices are not possible without reliable phase stability information over a wide range of temperatures. Furthermore, more modern techniques such as sinter forging [166] and severe plastic deformation [167] could be brought to bear on multifunctional materials allowing for an even greater degree of structural and functional property tuning.

Conclusions

Of the 180 ternary alloy systems reviewed, Heusler (Cu_2MnAl prototype) intermetallic compounds have been reported in 9 iron-based systems, 30 cobalt-based systems and 27 nickel-based systems. First principles calculations predict Heusler stability in 17 iron-based systems, 30 cobalt-based systems and 8 nickel-based systems. In the Ni-base systems, many more Heusler compounds have been reported than predicted, but in general, the difference from the predicted hull energy is small, often less than 1 kJ/mol. On the contrary, few iron-based systems are reported to have a Heusler compound while many more are predicted. The more commonly reported structure in the Iron-based systems is the B2 (CsCl prototype) structure. There remains the possibility that the Cu_2MnAl prototype structure could exist at lower temperatures or after longer annealing times that allow the additional ordering to take place. In addition, it can be difficult to distinguish between the B2 and $L2_1$ structures in some cases.

The state of order is rarely investigated or reported in papers dealing with property investigations of Heusler compounds and yet this is important in determining the properties, as is the precise composition. It may be possible to synthesize Heusler compounds that are predicted to be metastable through the use of non-equilibrium processing techniques.

We have identified the need for additional experimental phase diagram work in the following ternary systems: Co–Fe–Si, Co–Fe–Al, Co–Ta–Z (Z = Al, Ga, In, Si, Ge, Sn), Ni–Cr–Al, Ni–Mn–Ga, Ni–Mn–Ge, Ni–Mn–Sn, Fe–Ta–Ga, Fe–Co–Ga, Fe–Cu–Ga, Fe–Mn–Al, Fe–Ta–Ge, Fe–X–Si (X = V, Cr, Mn), Fe–Hf–Sn and all of the Fe–X–In systems.

The compounds Co_2ZrGa, Co_2ZrIn, Co_2TiIn, Co_2HfIn and Co_2VGe are predicted stable by ab initio calculations but have not been reported experimentally.

Compliance with ethical standards

Conflict of interest The authors declare that they have no conflict of interest.

References

1. Heusler F (1903) On magnetic manganese alloys. Verhandl Deuts Phys Ges 5:219
2. Graf T, Felser C, Parkin SSP (2011) Simple rules for the understanding of Heusler compounds. Prog Solid State Chem 39:1–50. doi:10.1016/j.progsolidstchem.2011.02.001
3. Siewert M, Gruner ME, Dannenberg A, Chakrabarti A, Herper HC, Wuttig M, Barman SR, Singh S, Al-Zubi A, Hickel T, Neugebauer J, Gillessen M, Dronskowski R, Entel P (2011) Designing shape-memory Heusler alloys from first-principles. Appl Phys Lett 99:191904. doi:10.1063/1.3655905
4. Galanakis I, Mavropoulos P, Dederichs PH (2005) Introduction to half-metallic Heusler alloys: electronic structure and magnetic properties. J Phys D, Appl Phys 39:765–775. doi:10.1088/0022-3727/39/5/S01
5. Balke B, Wurmehl S, Fecher GH (2008) Rational design of new materials for spintronics: Co_2FeZ (Z = Al, Ga, Si, Ge). Sci Technol Adv Mater. doi:10.1063/1.4821125
6. Kimura T, Hashimoto N, Yamada S, Miyao M, Hamaya K (2012) Room-temperature generation of giant pure spin currents using epitaxial Co_2FeSi spin injectors. NPG Asia Mater 4:e9
7. Kimura Y, Chai Y-W (2015) Ordered structures and thermoelectric properties of MNiSn (M = Ti, Zr, Hf)-based half-Heusler compounds affected by close relationship with Heusler compounds. JOM 67:233–245. doi:10.1007/s11837-014-1233-3
8. Nakatani T, Gercsi Z, Rajanikanth A, Takahashi Y, Hono K (2008) The effect of iron addition on the spin polarization and magnetic properties of Co_2CrGa Heusler alloy. J Phys Appl Phys 41:225002
9. Yin M, Chen S, Nash P (2013) Enthalpies of formation of selected Co_2YZ Heusler compounds. J Alloys Compd 577:49–56. doi:10.1016/j.jallcom.2013.04.136
10. Yin M, Nash P, Chen S, Du Y (2015) Enthalpies of formation of selected Fe_2YZ Heusler compounds. Intermetallics 57:34–40. doi:10.1016/j.intermet.2014.10.001
11. TPTC Thermodynamics Database. https://tptc.iit.edu/index.php/thermodynamics. Accessed 17 June 2015
12. Zhang L, Wang J, Du Y, Hu R, Nash P, Lu X-G, Jiang C (2009) Thermodynamic properties of the Al–Fe–Ni system acquired via a hybrid approach combining calorimetry, first-principles and CALPHAD. Acta Mater 57:5324–5341
13. Saal JE, Kirklin S, Aykol M, Meredig B, Wolverton C (2013) Materials design and discovery with high-throughput density functional theory: the open quantum materials database (OQMD). JOM 65:1501–1509. doi:10.1007/s11837-013-0755-4
14. Jain A, Ong SP, Hautier G, Chen W, Richards WD, Dacek S, Cholia S, Gunter D, Skinner D, Ceder G, Persson KA (2013) Commentary: the Materials Project: a materials genome approach to accelerating materials innovation. APL Mater 1:011002–011012. doi:10.1063/1.4812323
15. Aflow—Automatic—FLOW for materials discovery. http://www.aflowlib.org/. Accessed 31 May 2015
16. Calderon CE, Plata JJ, Toher C, Oses C, Levy O, Fornari M, Natan A, Mehl MJ, Hart G, Nardelli MB (2015) The AFLOW standard for high-throughput materials science calculations. ArXiv Prepr. http://arxiv.org/ArXiv150600303
17. Curtarolo S, Setyawan W, Wang S, Xue J, Yang K, Taylor RH, Nelson LJ, Hart GL, Sanvito S, Buongiorno-Nardelli M (2012) AFLOWLIB. ORG: a distributed materials properties repository from high-throughput ab initio calculations. Comput Mater Sci 58:227–235
18. Curtarolo S, Setyawan W, Hart GL, Jahnatek M, Chepulskii RV, Taylor RH, Wang S, Xue J, Yang K, Levy O (2012) AFLOW: an automatic framework for high-throughput materials discovery. Comput Mater Sci 58:218–226
19. Helmholdt RB, Buschow KHJ (1987) Crystallographic and magnetic structure of Ni_2MnSn and $NiMn_2Sn$. J Common Met 128:167–171. doi:10.1016/0022-5088(87)90202-5
20. Nazmunnahar M, Ryba T, del Val JJ, Ipatov M, González J, Hašková V, Szabó P, Samuely P, Kravcak J, Vargova Z, Varga R (2015) Half-metallic Ni_2MnSn Heusler alloy prepared by rapid quenching. J Magn Magn Mater 386:98–101. doi:10.1016/j.jmmm.2015.03.066
21. Dan NH, Duc NH, Yen NH, Thanh PT, Bau LV, An NM, Anh DTK, Bang NA, Mai NT, Anh PK, Thanh TD, Phan TL, Yu SC (2015) Magnetic properties and magnetocaloric effect in Ni–Mn–Sn alloys. J Magn Magn Mater 374:372–375. doi:10.1016/j.jmmm.2014.08.061
22. Marcinkowski MJ, Fisher RM (1963) Theoretical analysis of plastic deformation in superlattices based on the body-centered cubic structure. J Appl Phys 34:2135. doi:10.1063/1.1702703
23. Kawaharada Y, Kurosaki K, Yamanaka S (2003) High temperature thermoelectric properties of $(Fe_{1-x}V_x)_3$ Al Heusler type compounds. J Alloys Compd 349:37–40
24. Takeuchi T, Terazawa Y, Furuta Y, Yamamoto A, Mikami M (2013) Effect of heavy element substitution and off-stoichiometric composition on thermoelectric properties of Fe_2VAl-based Heusler phase. J Electron Mater 42:2084–2090
25. Skoug EJ, Zhou C, Pei Y, Morelli DT (2009) High thermoelectric power factor near room temperature in full-Heusler alloys. J Electron Mater 38:1221–1223. doi:10.1007/s11664-008-0626-x
26. Mikami M, Ozaki K, Takazawa H, Yamamoto A, Terazawa Y, Takeuchi T (2013) Effect of Ti substitution on thermoelectric properties of W-doped Heusler Fe_2VAl alloy. J Electron Mater 42:1801–1806. doi:10.1007/s11664-012-2433-7
27. Felser C, Wollmann L, Chadov S, Fecher GH, Parkin SSP (2015) Basics and prospective of magnetic Heusler compounds. APL Mater 3:041518–041519. doi:10.1063/1.4917387
28. Graf T, Parkin SS, Feiser C (2011) Heusler compounds—a material class with exceptional properties. IEEE Trans Magn 47:367–373
29. Felser C, Fecher GH, Balke B (2007) Spintronics: a challenge for materials science and solid-state chemistry. Angew Chem Int Ed 46:668–699. doi:10.1002/anie.200601815
30. Planes A, Mañosa L, Acet M (2009) Magnetocaloric effect and its relation to shape-memory properties in ferromagnetic Heusler alloys. J Phys: Condens Matter 21:233201–233229. doi:10.1088/0953-8984/21/23/233201
31. Wang C, Meyer J, Teichert N, Auge A, Rausch E, Balke B, Hütten A, Fecher GH, Felser C (2014) Heusler nanoparticles for spintronics and ferromagnetic shape memory alloys. J Vac Sci Technol B Microelectron Nanometer Struct 32:020802–020814. doi:10.1116/1.4866418
32. Buschow KHJ, van Engen PG, Jongebreur R (1983) Magneto-optical properties of metallic ferromagnetic materials. J Magn Magn Mater 38:1–22. doi:10.1016/0304-8853(83)90097-5
33. Lisenko LA, Ban Z, Gladyshevskii EI (1971) Investigation of the system Zr-Fe-Si. Croat Chem Acta 43:113–118
34. Miyawaki T, Foerster M, Finizio S, Vaz CAF, Mawass MA, Inagaki K, Fukatani N, Le Guyader L, Nolting F, Ueda K, Asano H, Kläui M (2013) The effect of magnetocrystalline anisotropy

on the domain structure of patterned Fe_2CrSi Heusler alloy thin films. J Appl Phys 114:073905. doi:10.1063/1.4818800
35. Suzuki RO, Kyono T (2004) Thermoelectric properties of Fe_2 TiAl Heusler alloys. J Alloys Compd 377:38–42. doi:10.1016/j.jallcom.2004.01.035
36. Palm M, Inden G, Thomas N (1995) The Fe-A1-Ti system. J Phase Equilibria 16:209–222
37. Markiv VY, Burnasheva VV, Ryabov VR (1973) Investigation of the systems Ti-Fe-Al, Ti-Ni-Al and Ti-Cu-Al. Metallofiz Akad Nauk Ukr SSR Inst Metallofiz 46:103–109
38. Ghosh G (1992) Aluminium-iron-titanium. Ternary alloys. VCH Verlagsgesellschaft Weinh Ger 5:456–469
39. Markiv VY, Hladyshevsky EI, Kzuma YB (1962) New ternary compounds with a structure of the $MnCu_2Al$ type. Dop Akad Nauk Ukrain RSR 1329–1331
40. Niculescu V, Budnick JI (1977) Limits of solubility, magnetic properties and electron concentration in $Fe_{3-x}T_xSi$ system. Solid State Commun 24:631–634. doi:10.1016/0038-1098(77)90378-7
41. Niculescu V, Burch TJ, Raj K, Budnick JI (1977) Properties of Heusler-type materials Fe_2TSi and $FeCo_2Si$. J Magn Magn Mater 5:60–66
42. Krez J, Balke B, Felser C, Hermes W, Schwind M (2015) Long-term stability of phase-separated half-Heusler compounds. ArXiv Prepr. http://arxiv.org/ArXiv150201828
43. Kuentzler R, Clad R, Schmerber G, Dossmann Y (1992) Gap at the Fermi level and magnetism in RMSn ternary compounds (R = Ti, Zr, Hf and M = Fe Co, Ni). J Magn Magn Mater 104–107:1976–1978. doi:10.1016/0304-8853(92)91629-8
44. Mikami M, Matsumoto A, Kobayashi K (2008) Synthesis and thermoelectric properties of microstructural Heusler Fe_2VAl alloy. J Alloys Compd 461:423–426. doi:10.1016/j.jallcom.2007.07.004
45. Mikami M, Kobayashi K, Kawada T, Kubo K, Uchiyama N (2009) Development of a thermoelectric module using the Heusler alloy Fe_2VAl. J Electron Mater 38:1121–1126. doi:10.1007/s11664-009-0724-4
46. Mikami M, Mizoshiri M, Ozaki K, Takazawa H, Yamamoto A, Terazawa Y, Takeuchi T (2014) Evaluation of the thermoelectric module consisting of W-doped Heusler Fe_2VAl alloy. J Electron Mater 43:1922–1926
47. Maebashi T, Kozakai T (2004) Doi M Phase equilibria in iron-rich Fe–Al–V ternary alloy system. Z Für Met 95:1005–1010. doi:10.3139/146.018048
48. Raghavan V (1992) The Fe-Ga-V (iron-gallium-vanadium) system. Phase Diagr Ternary Iron Alloys Indian Inst Met Calcutta India 6B:856–859
49. Fujii S, Ishida S, Asano S (1994) Electronic and magnetic properties of $X_2Mn_{1-x}V_xSi$ (X = Fe and Co). J Phys Soc Jpn 63:1881–1888. doi:10.1143/JPSJ.63.1881
50. Wurmehl S, Fecher GH, Felser C (2006) Co_2CrIn: a further magnetic Heusler compound. Z Naturforsch 61:749–752
51. Dai X, Liu G, Li Y, Qu J, Li J, Chen J, Wu G (2007) Structure and magnetic properties of highly ordered Co_2NiGa alloys. J Appl Phys 101:09N503. doi:10.1063/1.2709417
52. Markiv VY, Storozhenko AI (1974) Phase equilibria in the Zr-Fe-Ga and Zr-Co-Ga systems. Dopovidi Akad Nauk Ukr RSR Seriya Fiz-Tekhnichni Ta Mat Nauki 10:945–949
53. Belyavina NN, Markiv VY (1978) The Hf-Co-Ga system. Dopov Akad Nauk A 4:362–365
54. Markiv VY, Storozhenko AI, Zozulya AA (1974) Investigation of Ti-Fe-Ga and Ti-Co-Ga systems. Dopovidi Akad Nauk Ukr RSR Seriya Fiz-Tekhnichni Ta Mat Nauki 36:759–762
55. Ducher R, Kainuma R, Ohnuma I, Ishida K (2007) Phase equilibria and stability of B2 and $L2_1$ ordered phases in the Co–Fe–Ga Heusler alloy system. J Alloys Compd 437:93–101. doi:10.1016/j.jallcom.2006.07.091
56. Kobayashi K, Kainuma R, Fukamichi K, Ishida K (2005) Phase equilibria and stability of B2 and $L2_1$ ordered phases in the vicinity of half-metallic composition of Co–Cr–Ga Heusler alloy system. J Alloys Compd 403:161–167. doi:10.1016/j.jallcom.2005.05.009
57. Minakuchi K, Umetsu RY, Kobayashi K, Nagasako M, Kainuma R (2015) Phase equilibria and magnetic properties of Heusler-type ordered phases in the Co-Mn-Ga ternary system. J Alloys Compd 645:577–585. doi:10.1016/j.jallcom.2015.04.200
58. Ishikawa K, Kainuma R, Ohnuma I, Aoki K, Ishida K (2002) Phase stability of the X2AlTi (X: Fe Co, Ni and Cu) Heusler and B2-type intermetallic compounds. Acta Mater 50:2233–2243. doi:10.1016/S1359-6454(01)00434-7
59. Kim TW, Gambino RJ (1997) Temperature dependence of coercivity of the two-phase Co/Co_2TiSn magnet. J Appl Phys 81:5184–5186
60. Stadnyk Y, Romaka L, Horyn A, Tkachuk A, Gorelenko Y, Rogl P (2005) Isothermal sections of the Ti–Co–Sn and Ti–Co–Sb systems. J Alloys Compd 387:251–255
61. Skolozdra RV, Stadnyk YV, Gorelenko Y, Terletska EE (1990) Influence of vacancies on the magnetic and electrical properties of Heusler phases $Me'Co_{2-x}Sn(Me' = Ti, Zr, Hf)$. Phys Tverd Tela 32:1536–1538
62. Barth J, Fecher GH, Balke B, Graf T, Shkabko A, Weidenkaff A, Klaer P, Kallmayer M, Elmers H-J, Yoshikawa H (2011) Anomalous transport properties of the half-metallic ferromagnets Co_2TiSi, Co_2TiGe and Co_2TiSn. Philos Trans R Soc Lond Math Phys Eng Sci 369:3588–3601
63. Meinert M, Schmalhorst J, Wulfmeier H, Reiss G, Arenholz E, Graf T, Felser C (2011) Electronic structure of fully epitaxial Co_2TiSn thin films. Phys Rev B 83:064412
64. Lee SC, Lee TD, Blaha P, Schwarz K (2005) Magnetic and half-metallic properties of the full-Heusler alloys Co_2TiX (X = Al, Ga; Si, Ge, Sn; Sb). J Appl Phys 97:10C307
65. Webster PJ, Ziebeck KRA (1973) Magnetic and chemical order in Heusler alloys containing cobalt and titanium. J Phys Chem Solids 34:1647–1654
66. Ma Y, Heijl R, Palmqvist AE (2013) Composite thermoelectric materials with embedded nanoparticles. J Mater Sci 48:2767–2778. doi:10.1007/s10853-012-6976-z
67. Yin F, Tédenac J-C, Gascoigne F (2007) Thermodynamic modelling of the Ti–Sn system and calculation of the Co–Ti–Sn system. CALPHAD Comput Coupling Phase Diagr Thermochem 31:370–379
68. Kamiya N, Sakai T, Kainuma R, Ohnuma I, Ishida K (2004) Phase separation of BCC phase in the Co-rich portion of Co-Fe-Al system. Intermetallics 12:417–423
69. Kogachi M, Tadachi N, Nakanishi T (2006) Structural properties and magnetic behavior in Co–Fe–Al alloys. Intermetallics 14:742–749. doi:10.1016/j.intermet.2005.11.006
70. Balke B, Wurmehl S, Fecher GH, Felser C, Alves MCM, Bernardi F, Morais J (2007) Structural characterization of the Co_2FeZ (Z = Al, Si, Ga, and Ge) Heusler compounds by X-ray diffraction and extended X-ray absorption fine structure spectroscopy. Appl Phys Lett 90:172501–172504. doi:10.1063/1.2731314
71. Shreder EI, Svyazhin AD, Belozerova KA (2013) Optical properties of Heusler alloys Co_2FeSi, Co_2FeAl, Co_2CrAl, and Co_2CrGa. Phys Met Metallogr 114:904–909. doi:10.1134/S0031918X13110124
72. Colinet C, Inden G, Kikuchi R (1993) CVM calculation of the phase diagram of bcc Fe–Co–Al. Acta Metall Mater 41:1109–1118
73. Watson A, MSIT (2004) MSI Eureka Evaluation Report 10.15955.2.8 System Name: Al–Co–Fe. MSIT® Registered. Trademark MSI, Materials Science International Services GmbH

74. Kozakai T, Miyazaki T (1994) Experimental and theoretical studies on phase separations in the Fe–Al–Co ordering alloy system. J Mater Sci 29:652–659. doi:10.1007/BF00445974
75. Kozakai T, Okamoto R, Miyazaki T (1999) Phase equilibria in the Fe-Al-Co ternary system at 923 K. Z Für Met 90:261–266
76. Takamura Y, Nakane R, Sugahara S (2009) Analysis of $L2_1$-ordering in full-Heusler Co_2FeSi alloy thin films formed by rapid thermal annealing. J Appl Phys 105:07B109. doi:10.1063/1.3075989
77. Yamada S, Hamaya K, Yamamoto K, Murakami T, Mibu K, Miyao M (2010) Significant growth-temperature dependence of ferromagnetic properties for Co_2FeSi/Si(111) prepared by low-temperature molecular beam epitaxy. Appl Phys Lett 96:082511. doi:10.1063/1.3330895
78. Blum CGF, Jenkins CA, Barth J, Felser C, Wurmehl S, Friemel G, Hess C, Behr G, Büchner B, Reller A, Riegg S, Ebbinghaus SG, Ellis T, Jacobs PJ, Kohlhepp JT, Swagten HJM (2009) Highly ordered, half-metallic Co_2FeSi single crystals. Appl Phys Lett 95:161903–161904. doi:10.1063/1.3242370
79. Kasahara K, Yamamoto K, Yamada S, Murakami T, Hamaya K, Mibu K, Miyao M (2010) Highly ordered Co_2FeSi Heusler alloys grown on Ge(111) by low-temperature molecular beam epitaxy. J Appl Phys 107:09B105. doi:10.1063/1.3350915
80. Garg AB, Vijayakumar V (2011) Phase stability of Heusler compound Co_2FeSi under pressure: an in situ X-ray diffraction investigation. J Appl Phys 110:083523. doi:10.1063/1.3656983
81. Bombor D, Blum CGF, Volkonskiy O, Rodan S, Wurmehl S, Hess C, Büchner B (2013) Half-Metallic ferromagnetism with unexpectedly small spin splitting in the Heusler compound Co_2FeSi. Phys Rev Lett 110:066601–066605. doi:10.1103/PhysRevLett.110.066601
82. Kiss LF, Bortel G, Bujdosó L, Kaptás D, Kemény T, Vincze I (2015) Average magnetization and Fe hyperfine fields in Co_2FeSi-based Heusler alloys. Acta Phys Pol A 127:347–349. doi:10.12693/APhysPolA.127.347
83. Hashimoto M, Herfort J, Schönherr HP, Ploog KH (2005) Epitaxial Heusler alloy Co_2FeSi/GaAs(001) hybrid structures. Appl Phys Lett 87:102506. doi:10.1063/1.2041836
84. Fecher GH, Kandpal HC, Wurmehl S, Felser C, Schönhense G (2006) Slater–Pauling rule and Curie temperature of Co_2-based Heusler compounds. J Appl Phys 99:08J106. doi:10.1063/1.2167629
85. Wurmehl S, Fecher GH, Kandpal HC, Ksenofontov V, Felser C, Lin H-J, Morais J (2005) Geometric, electronic, and magnetic structure of Co_2FeSi: Curie temperature and magnetic moment measurements and calculations. Phys Rev B 72:184434–184439. doi:10.1103/PhysRevB.72.184434
86. Gercsi Z, Hono K (2007) Ab initio predictions for the effect of disorder and quaternary alloying on the half-metallic properties of selected Co_2Fe-based Heusler alloys. J Phys: Condens Matter 19:326216. doi:10.1088/0953-8984/19/32/326216
87. Mohankumar R, Ramasubramanian S, Rajagopalan M, Raja MM, Kamat SV, Kumar J (2015) Density functional study of half-metallic property on B2 disordered Co_2FeSi. J Mater Sci 50:1287–1294. doi:10.1007/s10853-014-8687-0
88. Chen X-Q, Podloucky R, Rogl P (2006) Ab initio prediction of half-metallic properties for the ferromagnetic Heusler alloys Co_2MSi (M = Ti, V, Cr). J Appl Phys 100:113901
89. Balke B, Fecher GH, Kandpal HC, Felser C, Kobayashi K, Ikenaga E, Kim J-J, Ueda S (2006) Properties of the quaternary half-metal-type Heusler alloy $Co_2Mn_{1x}Fe_xSi$. Phys Rev B 74:104405–104410. doi:10.1103/PhysRevB.74.104405
90. Yin M, Nash P, Chen S (2013) Heat capacities of several Co_2YZ Heusler compounds. Thermochim Acta 574:79–84. doi:10.1016/j.tca.2013.10.004
91. Raynor GV, Rivlin VG (1988) Co–Fe–Si Phase equilibria of iron ternary alloys. Institute of Metals, London, pp 256–267
92. Rokhlin L, MSIT® (2007) Co–Fe–Si ternary phase diagram evaluation. MSI Eureka Evaluation Report 10.10292.1.2. MSI Eureka
93. Raghavan V (1987) The Co–Fe–Sn (cobalt–iron–tin) system. Phase diagram. Ternary iron alloys. Indian Institute of Metals, Calcutta, pp 23–30
94. Singh VK, Singh M, Bahn S (1985) Phase transformation studies on Fe–Co–Sn alloys. Trans Indian Inst Met 38:128–131
95. Zhang W, Jiko N, Mibu K, Yoshimura K (2005) Effect of substitution of Mn with Fe or Cr in Heusler alloy of Co_2MnSn. J Phys: Condens Matter 17:6653–6662. doi:10.1088/0953-8984/17/42/006
96. Li T, Duan J, Yang C, Kou X (2013) Synthesis, microstructure and magnetic properties of Heusler Co_2FeSn nanoparticles. Micro Nano Lett IET 8:143–146. doi:10.1049/mnl.2012.0905
97. Duan J, Kou X (2013) Effect of current density on the microstructure and magnetic properties of electrodeposited Co_2FeSn Heusler alloy. J Electrochem Soc 160:D471–D475. doi:10.1149/2.089310jes
98. Tanaka MA, Ishikawa Y, Wada Y, Hori S, Murata A, Horii S, Yamanishi Y, Mibu K, Kondou K, Ono T, Kasai S (2012) Preparation of Co_2FeSn Heusler alloy films and magnetoresistance of Fe/MgO/Co_2FeSn magnetic tunnel junctions. J Appl Phys 111:053902–053906. doi:10.1063/1.3688324
99. Watanabe N, Sano K, Tasugi N, Yamaguchi T, Yamamoto A, Ueno M, Sumiyoshi R, Arakawa T, Koiwa I (2015) Preparation of Co_2FeSn Heusler alloys by electrodeposition method. APL Mater 3:041804. doi:10.1063/1.4918639
100. Alijani V, Winterlik J, Fecher GH, Naghavi SS, Chadov S, Gruhn T, Felser C (2012) Quaternary Heusler compounds $Co_{2-x}Rh_xMnZ$ (Z = Ga, Sn, Sb): crystal structure, electronic structure, and magnetic properties. J Phys: Condens Matter 24:046001–046008. doi:10.1088/0953-8984/24/4/046001
101. Nazmunnahar M, González L, Ilyn M, del Val JJ, Suño JJ, Hernando B, González J (2012) Structural and magnetization changes at high temperature in $Co_{50}Mn_{30}In_{20}$ alloy. J Nanosci Nanotechnol 12:7442–7445
102. Gladyshevskii EI (1962) Crystal structure of compounds and phase equilibria in ternary systems of two transition metals and silicon. Sov Powder Metall Met Ceram Transl Poroshkovaya Metall Kiev 1:262–265
103. Dovbenko O, Stein F, Palm M, Prymak O (2010) Experimental determination of the ternary Co–Al–Nb phase diagram. Intermetallics 18:2191–2207. doi:10.1016/j.intermet.2010.07.004
104. Palm M, He C, Dovbenko O, Stein F (2012) Liquidus projection and reaction scheme of the Co–Al–Nb system. J Phase Equilibria. doi:10.1088/0022-3727/46/47/475001
105. He C, Stein F, Palm M (2015) Thermodynamic description of the systems Co–Nb, Al–Nb and Co–Al–Nb. J Alloys Compd 637:361–375. doi:10.1016/j.jallcom.2015.02.182
106. Carbonari AW, Saxena RN, Pendl W, Mestnik Filho J, Attili RN, Olzon-Dionysio M, De Souza SD (1996) Magnetic hyperfine field in the Heusler alloys Co_2YZ (Y = V, Nb, Ta, Cr; Z = Al, Ga). J Magn Magn Mater 163:313–321
107. Kerkau A, Kreiner G (2010) Crystal structure of niobium aluminium cobalt, Nb $(Al_{0.62}Co_{0.38})_2$. Z Für Krist-New Cryst Struct 225:621–622
108. Skolozdra RV, Okhrimovich KO (1971) The Nb–Co–Sn and Nb–Ni–Sn systems. Russ Metall Transl Izv Akad Nauk SSSR Met 6:135–138
109. Bardos DI, Beck PA (1966) Electron phases in certain ternary alloys of transition metals with silicon. Trans Metall Soc AIME 236:64–69
110. Hunt CR Jr, Raman A (1968) Alloy chemistry of σ, β-related phases I. Extension of μ and occurance of μ-phases in the ternary systems Nb (Ta)–X–Al (X = Fe Co, Ni, Cu, Cr, Mo). Z Met 59:701–707

111. Markiv VY, Voroshilov YV, Krypyakevych PI, Cherkashin EE (1964) New compounds of the $MnCu_2Al$ and $MgZn_2$ types containing aluminum and gallium. Sov Phys Crystallogr Transl Krist 9:619–620
112. Gladyshevskii EI, Kuz'ma YB (1958) The crystal structure of ternary compounds in Co–Mn–Ge and Ni–Mn–Ge systems. Visnik Vivskogo Derzhavnogo Univ Seriya Khimichna 5:115–117
113. Lee YP, Kim RJ, Yoo YJ, Kim KW, Kudryavtsev YV (2006) Spin-photonic, photonic and other relevant properties of Ni 2 MnGe and other Heusler alloys. J Korean Phys Soc. 49(95):2080–2083
114. Marazza R, Rambaldi G, Ferro R (1974) Ternary intermetallic phases of the cesium chloride or aluminum-copper-manganese ($AlCu_2Mn$) structure type have related 1:1:2 stoichiometries. Atti Della Accad Nazioale Dei Lincei Cl Sci Fis Mat 55(5):518–521
115. Cherkashyn EE, Gladyshevskii EI, Kuz'ma YB (1958) X-ray structural study of some systems of the transition metals. Zh Neorg Khim 3:650–653
116. Kuz'ma YB, Gladyshevskii EI, Teslyuk MY (1963) Crystal structure of $Mn_6Ni_{16}Ge_7$. Visn Lviv Derzh Univ Ser Khim 6:54–57
117. Zayak AT, Entel P (2005) A critical discussion of calculated modulated structures, Fermi surface nesting and phonon softening in magnetic shape memory alloys $Ni_2Mn(Ga, Ge, Al)$ and $Co_2Mn(Ga, Ge)$. J Magn Magn Mater 290–291:874–877. doi:10.1016/j.jmmm.2004.11.401
118. Buschow KHJ, Van Engen PG (1981) Magnetic and magneto-optical properties of Heusler alloys based on aluminium and gallium. J Magn Magn Mater 25:90–96
119. Oforka NC, Harworth CW (1987) Phase equilibria of aluminium–chromium–nickel system. Scand J Met 16:184–188
120. Cutler RW (2011) The 1200 °C isothermal sections of the Ni–Al–Cr and the Ni–Al–Mo ternary phase diagrams. Doctoral Dissertation, The Ohio State University
121. Zhang W, Qian Z, Tang J, Zhao L, Sui Y, Wang H, Li Y, Su W, Zhang M, Liu Z (2007) Superparamagnetic behaviour in melt-spun Ni_2FeAl ribbons. J Phys: Condens Matter 19:096214
122. Ducher R, Kainuma R, Ishida K (2008) Phase equilibria in the Ni–Fe–Ga alloy system. J Alloys Compd 463:213–219. doi:10.1016/j.jallcom.2007.09.079
123. Zhang HR, Ma C, Tian HF, Wu GH, Li JQ (2008) Martensitic transformation of Ni_2FeGa ferromagnetic shape-memory alloy studied via transmission electron microscopy and electron energy-loss spectroscopy. Phys Rev B 77:214106
124. Oikawa K, Ota T, Imano Y, Omori T, Kainuma R, Ishida K (2006) Phase equilibria and phase transformation of Co–Ni–Ga ferromagnetic shape memory alloy system. J Phase Equilibria Diffus 27:75–82. doi:10.1361/105497106X92835
125. Ghosh G (2013) Cu–Ni–Sn ternary phase diagram evaluation. Effenberg G Ed MSI Eureka MSI, Materials Science International Services GmbH, Stuttgart. pp 303–337
126. Stadnyk YV, Skolozdra RV (1991) Isothermal section of the system Ti–Ni–Sn at 770 K. Izv USSR Neorg Mater 27:2209–2210
127. Stadnyk YV, Skolozdra RV (1994) Phase structure of Zr–Ni–Sn <50 % at Sn at 800° and >50 % at Sn at 600°. Metally 26:164–167
128. Stadnyk YV, Romaka LP (2001) Phase equilibria in the Hf–Ni–Sn ternary system and crystal structure of the Hf_2Ni_2Sn compound. J Alloys Compd 316:169–171
129. Kenjo T, Kimura Y, Mishima Y (2010) Phase stability and thermoelectric properties of half Heusler compounds. Mater Res Soc Symp Proc 1218:43–48
130. Populoh S, Aguirre MH, Brunko OC, Galazka K, Lu Y, Weidenkaff A (2012) High figure of merit in (Ti, Zr, Hf) NiSn half-Heusler alloys. Scr Mater 66:1073–1076
131. Makongo JPA, Misra DK, Zhou X, Pant A, Shabetai MR, Su X, Uher C, Stokes KL, Poudeu PFP (2011) Simultaneous large enhancements in thermopower and electrical conductivity of Bulk nanostructured half-Heusler alloys. J Am Chem Soc 133:18843–18852. doi:10.1021/ja206491j
132. Koizumi Y, Ro Y, Nakazawa S, Harada H (1997) NiTi-base intermetallic alloys strengthened by Al substitution. Mater Sci Eng A 223:36–41
133. Jung J, Ghosh G, Olson GB (2003) A comparative study of precipitation behavior of Heusler phase (Ni_2TiAl) from B2–TiNi in Ni–Ti–Al and Ni–Ti–Al–X (X = Hf, Pd, Pt, Zr) alloys. Acta Mater 51:6341–6357. doi:10.1016/j.actamat.2003.08.003
134. Liebscher CH, Radmilovic V, Dahmen U, Asta M, Ghosh G (2013) On the formation of hierarchically structured $L2_1$-Ni_2-TiAl type precipitates in a ferritic alloy. J Mater Sci 48:2067–2075. doi:10.1007/s10853-012-6980-3
135. Polvani RS, Strutt PR, Tzeng W (1976) High-intrinsic creep strength of non-stoichiometric nickel-aluminum-titanium (Ni_2 AlTi). Thirty-Fourth Annual Electron Microscopy Society of American Meeting, vol. 34, pp 594–595
136. Kaufman L, Nesor H (1974) Calculation of superalloy phase diagrams: Part II. Metall Trans 5:1623–1629
137. Ziebeck K, Neumann K-U (2001) Ni-Hf-Al. In: Alloys Compd. -Elem. Main Group Elem. Part 2. Springer, pp 72–76
138. Garg A, Raj SV, Noebe RD, Nathal MV, Darolia R (1998) Plastic instability during creep deformation of a NiAl–Hf single-crystal alloy—a case study. Metall Mater Trans A 29:179–189
139. Whittenberger JD, Locci IE, Darolia R, Bowman R (1999) 1300 K creep behavior of [001] oriented Ni–49Al–1Hf (at.%) single crystals. Mater Sci Eng, A 268:165–183
140. Cui CY, Guo JT, Ye HQ (2006) Precipitation behavior of Heusler phase (Ni_2AlHf) in multiphase NiAl alloy. J Mater Sci 41:2981–2987. doi:10.1007/s10853-006-6732-3
141. Cornish L, Cupid D, Gröbner J, Malfliet A (2009) Al–Nb–Ni ternary phase diagram evaluation. MSI Eureka Effenberg G Ed MSI, Materials Science International Service GmbH, Stuttgart
142. Zakharov A (1993) Aluminum–nickel–tantalum. In: Petzow G, Effenberg G (eds) Ternary alloys, vol 7. Springer, New York, pp 483–497
143. Stearns MB (1978) Conduction electron polarization and moment perturbations in dilute Fe_3Si based alloys. J Appl Phys 49:1555–1557
144. Reitz JR, Stearns MB (1979) Theory of spin wave spectra in Heusler alloys. J Appl Phys 50:2066–2068
145. Kübler J, William AR, Sommers CB (1983) Formation and coupling of magnetic moments in Heusler alloys. Phys Rev B 28:1745
146. Prasad RVS, Phanikumar G (2009) Amorphous and nano crystalline phase formation in Ni_2MnGa ferromagnetic shape memory alloy synthesized by melt spinning. J Mater Sci 44:2553–2559. doi:10.1007/s10853-009-3333-y
147. Mukadam MD, Yusuf SM, Bhatt P (2013) Tuning the magnetocaloric properties of the $Ni_{2+x}Mn_{1-x}Sn$ Heusler alloys. J Appl Phys 113:3911
148. Kainuma R, Ise M, Ishikawa K, Ohnuma I, Ishida K (1998) Phase equilibria and stability of the B2 phase in the Ni–Mn–Al and Co–Mn–Al systems. J Alloys Compd 269:173–180
149. Millán JN, Sandlöbes S, Al-Zubi A, Hickel T, Choi P, Neugebauer J, Ponge D, Raabe D (2014) Designing Heusler nanoprecipitates by elastic misfit stabilization in Fe–Mn maraging steels. Acta Mater 76:94–105. doi:10.1016/j.actamat.2014.05.016

150. Miyamoto T, Nagasako M, Kainuma R (2013) Phase equilibria in the Ni–Mn–In alloy system. J Alloys Compd 549:57–63. doi:10.1016/j.jallcom.2012.08.128
151. Banik S, Singh S, Rawat R, Mukhopadhyay PK, Ahuja BL, Awasthi AM, Barman SR, Sampathkumaran EV (2009) Variation of magnetoresistance in Ni_2Mn Ga with composition. J Appl Phys 106:103919
152. Babita I, Raja MM, Gopalan R, Chandrasekaran V, Ram S (2007) Phase transformation and magnetic properties in Ni–Mn–Ga Heusler alloys. J Alloys Compd 432:23–29
153. Cherechukin AA, Takagi T, Matsumoto M, Buchel'Nikov VD (2004) Magnetocaloric effect in $Ni_{2+x}Mn_{1-x}Ga$ Heusler alloys. Phys Lett A 326:146–151
154. Pons J, Chernenko VA, Santamarta R, Cesari E (2000) Crystal structure of martensitic phases in Ni–Mn–Ga shape memory alloys. Acta Mater 48:3027–3038
155. Zheng H, Wang W, Xue S, Zhai Q, Frenzel J, Luo Z (2013) Composition-dependent crystal structure and martensitic transformation in Heusler Ni–Mn–Sn alloys. Acta Mater 61:4648–4656
156. Chieda Y, Kanomata T, Fukushima K, Matsubayashi K, Uwatoko Y, Kainuma R, Oikawa K, Ishida K, Obara K, Shishido T (2009) Magnetic properties of Mn-rich Ni_2MnSn Heusler alloys under pressure. J Alloys Compd 486:51–54
157. Hu Q-M, Li C-M, Yang R, Kulkova SE, Bazhanov DI, Johansson B, Vitos L (2009) Site occupancy, magnetic moments, and elastic constants of off-stoichiometric Ni_2MnGa from first-principles calculations. Phys Rev B 79:144112
158. Wang X, Shang J-X, Wang F-H, Jiang C-B, Xu H-B (2014) The structural stability and magnetic properties of the ferromagnetic Heusler alloy Ni–Mn–Sn: a first principle investigation. J Magn Magn Mater 355:173–179. doi:10.1016/j.jmmm.2013.12.017
159. Xu N, Raulot JM, Li ZB, Bai J, Yang B, Zhang YD, Meng XY, Zhao X, Zuo L, Esling C (2015) Composition-dependent structural and magnetic properties of Ni–Mn–Ga alloys studied by ab initio calculations. J Mater Sci 50:3825–3834. doi:10.1007/s10853-015-8951-y
160. Ducher R, Kainuma R, Ishida K (2008) Phase equilibria in the Ni–Co–Ga alloy system. J Alloys Compd 466:208–213
161. Ishida K, Kainuma R, Ueno N, Nishizawa T (1991) Ductility enhancement in NiAl (B2)-base alloys by microstructural control. Metall Trans A 22:441–446
162. Oikawa K, Ota T, Gejima F, Ohmori T, Kainuma R, Ishida K (2001) Phase equilibria and phase transformations in new B2-type ferromagnetic shape memory alloys of Co–Ni–Ga and Co–Ni–Al systems. Mater Trans 42:2472–2475
163. Snyder GJ, Toberer ES (2008) Complex thermoelectric materials. Nat Mater 7:105–114
164. Li J-F, Liu W-S, Zhao L-D, Zhou M (2010) High-performance nanostructured thermoelectric materials. NPG Asia Mater 2:152–158. doi:10.1038/asiamat.2010.138
165. Birkel CS, Douglas JE, Lettiere BR, Seward G, Verma N, Zhang Y, Pollock TM, Seshadri R, Stucky GD (2013) Improving the thermoelectric properties of half-Heusler TiNiSn through inclusion of a second full-Heusler phase: microwave preparation and spark plasma sintering of $TiNi_{1+x}Sn$. Phys Chem Chem Phys 15:6990. doi:10.1039/c3cp50918d
166. Ur S-C, Nash P, Kim I-H (2004) Thermoelectric properties of Zn_4Sb_3 processed by sinter-forging. Mater Lett 58:2937–2941. doi:10.1016/j.matlet.2004.05.027
167. Zhilyaev AP, Langdon TG (2008) Using high-pressure torsion for metal processing: fundamentals and applications. Prog Mater Sci 53:893–979. doi:10.1016/j.pmatsci.2008.03.002
168. Villars P (2014) Material Phases Data System (MPDS), CH-6354 Vitznau, Switzerland; Springer Materials; c_0200229. http://materials.springer.com.ezproxy.gl.iit.edu/isp/phase-diagram/docs/c_0200229. Accessed 8 Apr 2015
169. Villars P (2014) Material Phases Data System (MPDS), CH-6354 Vitznau, Switzerland; Springer Materials; c_0975730. http://materials.springer.com.ezproxy.gl.iit.edu/isp/phase-diagram/docs/c_0975730. Accessed 8 Apr 2015
170. Seibold A (1981) Phasengleichgewichte in den ternären Systemen Ti–Fe–O und Ti–Al–Fe. Z Für Met 72:712–719
171. Villars P (2014) Material Phases Data System (MPDS), CH-6354 Vitznau, Switzerland; Springer Materials; c_0975731. http://materials.springer.com.ezproxy.gl.iit.edu/isp/phase-diagram/docs/c_0975731. Accessed 8 Apr 2015
172. Kazuhiro Ishikawa, Ryosuke Kainuma, Kiyohito Ishida, MSIT® MSI Eureka Evaluation Report 10.10909.2.9 System Name: Al–Co–Ti Report
173. Ishikawa K, Himuro Y, Ohnuma I, Kainuma R, Aoki K, Ishida K (2001) Phase equilibria in the Co–Ti portion of the Co–Al–Ti ternary system. J Phase Equilibria 22:219–226
174. Pierre Villars Al–Co–Ti Isothermal Section of Ternary Phase Diagram—Springer Materials. In: Mater. Phases Data Syst. MPDS. http://materials.springer.com.ezproxy.gl.iit.edu/isp/phase-diagram/docs/c_0200101. Accessed 4 Aug 2015
175. Villars P (2014) Material Phases Data System (MPDS), CH-6354 Vitznau, Switzerland; SpringerMaterials; c_0925091. http://materials.springer.com.ezproxy.gl.iit.edu/isp/phase-diagram/docs/c_0925091. Accessed 8 Apr 2015
176. Vogel R, Rosenthal K (1935) Das System Eisen-Kobalt-Kobaltsilizid-Eisensilizid. Arch Für Eisenhüttenwes 9:293–299
177. Belyavina NN, Markiv VY (1978) The Hf–Co–Ga system. Dopovidi Akad Nauk Ukr RSR Seriya Fiz-Mat Ta Tekhnichni Nauki 4:362–365
178. Villars P (2014) Material Phases Data System (MPDS), CH-6354 Vitznau, Switzerland; Springer Materials; c_0925212. http://materials.springer.com.ezproxy.gl.iit.edu/isp/phase-diagram/docs/c_0925212. Accessed 8 Apr 2015
179. Romaka VV, Rogl P, Romaka L, Stadnyk Y, Melnychenko N, Grytsiv A, Falmbigl M, Skryabina N (2013) Phase equilibria, formation, crystal and electronic structure of ternary compounds in Ti–Ni–Sn and Ti–Ni–Sb ternary systems. J Solid State Chem 197:103–112. doi:10.1016/j.jssc.2012.08.023